Air Shower Multi-Mesh Proportional Counter

Shahina
MS13002

A dissertation submitted for the partial fulfillment of BS-MS dual degree in Science

Under the guidance of
Dr. Satyajit Jena

April 2018

Indian Institute of Science Education and Research Mohali
Sector - 81, SAS Nagar, Mohali 140306, Punjab, India

Certificate of Examination

This is to certify that the dissertation titled **Air Shower Multi-Mesh Proportional Counter** submitted by **Shahina** (Reg. No. MS13002) for the partial fulfillment of BS-MS dual degree programme of the Institute, has been examined by the thesis committee duly appointed by the Institute. The committee finds the work done by the candidate satisfactory and recommends that the report be accepted.

Dr. Rajeev Kapri

Dr. Ananth Venkatesan

Dr. Satyajit Jena
(Supervisor)

Dated: 20.04.2018

Declaration

The work presented in this dissertation has been carried out by me under the guidance of Dr. Satyajit Jena at the Indian Institute of Science Education and Research Mohali.

This work has not been submitted in part or in full for a degree, a diploma, or a fellowship to any other university or institute. Whenever contributions of others are involved, every effort is made to indicate this clearly, with due acknowledgement of collaborative research and discussions. This thesis is a bonafide record of original work done by me and all sources listed within have been detailed in the bibliography.

Shahina
(Candidate)

Dated: April 20, 2018

In my capacity as the supervisor of the candidates project work, I certify that the above statements by the candidate are true to the best of my knowledge.

Dr. Satyajit Jena
(Supervisor)

Acknowledgement

I would like to express my sincere gratitude towards my guide Dr. Satyajit Jena for his elite guidance, ceaseless encouragement, and support throughout my research work. I thank him for giving time for me despite his extremely hectic schedule. I appreciate him for valuable physics discussions and critical proofreading of this thesis.

I would also like to thank my thesis committee members Dr. Rajeev Kapri and Dr. Ananth Venkatesan for their valuable suggestions and criticism of my work.

I am gratefully indebted to Rohit Gupta and Nishat Fiza for proofreading and for their very valuable comments on this thesis. I would like to mention my heartiest gratitude to all my lab members-Tasha, Anjaly, Asish, Akhil, Shubham and Neeraj.

I am indebted to Uddipan, Harleen, Ashima, Kushal, Jyoti and Shreya whose friendship has played an important role in my life. I thank them for being there for me and for their infinite love, encouragement, and support.

Above all, my deepest gratitude goes to my parents, brother, and all my relatives for their unlimited love, support, and encouragement. Finally, my deep respect for everybody who helped me in my personal and professional growth.

Finally, I am thankful to IISER Mohali for providing me infrastructure and Computer Centre for all the technical support. I would like to acknowledge DST INSPIRE, Government of India for the financial support.

Shahina
MS13002
IISER Mohali.

Abstract

In this work some properties of Multi-wire proportional counters using air as the ionizing gas medium at atmospheric pressure were described. We examined the use of MWPCs in the proportional mode, where an MWPC defines a small sensitive area (2.4 cm $\times$ 2.4 cm) which can be extended by adding more wires for large area detection. We examined the track of particles passing through this area in each shower and this was obtained from the amplitude of the pulse given by the MWPC at the time of the event. This information was used to calculate the timing resolution of the detector. MWPCs were assembled into a hexagonal array and were used to record the particles present in cosmic ray air showers. The entire simulation and calculations were done using various simulation packages .

Contents

List of Figures

Introduction

The development of particle detectors practically starts with the discovery of radioactivity by Henri Becquerel in the year 1896. The first radiation detection devices i.e., X-ray films were thus extremely simple. In the course of time, the measurement methods have been greatly refined. Today, it is insufficient only to detect particles and radiation. One would like to identify their nature as well. The particles in extensive air showers are divided into three principal components:

- Nuclear active component, which includes all kinds of particles that participate in strong nuclear interactions,
- The electromagnetic or soft component, consisting of photons, electrons, and positrons,
- The mu-meson component.

The most numerous particles remaining in the shower are the muons. Hence in order to detect muons, we convert its energy to a known measurable form. For example, when a charged particle or radiation passes through gas it loses its energy which can be collected in the form of an electrical signal by applying an electric field. Early measurements of the properties of air showers, such as relative numbers and energy spectra of the different kinds of secondary particles, were made with crude methods of shower selection. In the past mostly spark chambers were used to measure the trajectory of high energy particles and to identify their nature and energies. Since the successful operation of large area Multiwire proportional chambers (MWPC) by Charpak et al. [10] at CERN in 1968, these detectors have come into widespread use, and a significant amount of development work has been done in recent years.

This thesis is concerned with the use of MWPC (Multiwire Proportional Chambers) to detect the particles in air showers which will not only help us to know the behavior of high energy particles but also know more about their sources and space

through which they have propagated. They are more favorable in large area experiments because of the flexibility they offer. Apart from being inexpensive, these detectors provide good timing and position resolution and are insensitive to radiation damage. Their ease of fabrication into any shape and size is an added advantage. They have good rate handling capacities and parameters like operating voltages and gas pressures can be fully customized to detect particles. MWPC produces an electrical pulse when air shower particles pass through it. Today most fast detectors contain a large number of proportional chambers and their use has spread to many different fields of applied research as well such as X-ray and heavy ion astronomy, nuclear medicine and protein crystallography.

One of the most important measurements in high energy physics experiments - be it in elementary particle physics or in cosmic ray physics - is the exact determination of the trajectory of the particles under investigation. We want to know the track of the particle because it will help us to know the beam profile (cross-sectional distribution of the beam) once we know the track of each individual particle. This is highly relevant to high energy scattering experiments and high-energy particles like cosmic rays from astrophysical sources. In this thesis, we have simulated the track of the incoming particle. In reality, nobody knows the track of the particle beforehand. If we perform the actual experiment with the proposed detector we will get to know the track which was not known before by looking at the signal from the wires of the detector. In our work MWPC was also used to determine the timing resolution of the detector with respect to the arrival direction of the shower. Shower particle detectors which are composed of a medium similar to air have the advantage of measuring particle numbers with minimal interference. This advantage, however, is partly negated because the shower particles traversing such a detector necessarily have a small energy loss which is subject to relatively large fluctuations. A detailed study has been made on MWPC in this thesis on using air as the ionizing gas mixture at atmospheric pressure and compared its properties with that of the conventional gas mixture $CF_4/CO_2/Ar$ (10:50:40) used in LHCb experiment.

The thesis develops as follows: In Chapter 1, a short description of how radiation interacts with matter is given with a focus on the interaction of charged particles. The second chapter is devoted to properties of gas mixtures on how the electron and ion transport properties vary in different gas mixtures. In Chapter 3, computer tools used in gas detector simulation will be described and the following programs will be introduced: Heed, Magboltz, neBEM and Garfield. These programs calculate,

respectively particle energy loss and electron transport properties in gases, electric fields established in the chambers and final chamber performance.

In Chapters 4 and 5, the results of simulations of MWPC, its geometry and construction will be presented. The conclusions of this thesis work will also be given in chapter 5.

Chapter 1

Interaction of particles and radiations with matter

The operation of any detector basically depends on the manner in which the radiation to be detected interacts with the material of the detector itself. An understanding of the response of a specific detector must, therefore, be based on a familiarity with the fundamental mechanisms by which radiations interact with matter.

Particles and radiation can be detected only through their interactions with matter. There are specific interactions for charged particles which are different from those of neutral particles, e.g. of photons. Every interaction process can be used as a basis for a detector concept. The variety of these processes is quite rich and, as a consequence, a large number of detection devices for particles and radiation exist.

The main interactions of charged particles with matter are ionization and excitation. For relativistic particles, bremsstrahlung energy losses must also be considered. Neutral particles must produce charged particles in an interaction that are then detected via their characteristic interaction processes. In the case of photons, these processes are the photoelectric effect, Compton scattering and pair production of electrons. The electrons produced in these photon interactions can be observed through their ionization in the sensitive volume of the detector.

1.1 Interaction of heavy charged particles

Heavy charged particles, such as the alpha particles, interact with matter through Coulomb forces between their positive charge and the negative charge of the orbital electrons within the absorber atoms. Upon entering any absorbing medium,

the charged particle immediately interacts simultaneously with many electrons. In any one such encounter, the electron feels an impulse from the attractive coulomb force as the particle passes its vicinity. Depending on the proximity of the encounter, this impulse may be sufficient either to raise the electron to a higher-lying shell within the absorber atom (excitation) or to completely remove the electron from the atom (ionization). The energy that is transferred to the electron must come at the expense of the charged particle, and its velocity is therefore decreased as a result of the encounter. The maximum energy T_{max} transferred in a single collision from the particle of mass m_0 and reduced velocity $\beta = \frac{v}{c}$ to an electron of mass $m_e << m_0$ is :

$$T_{max} = \frac{2m_e c^2 \beta^2 \gamma^2}{1 + 2\gamma \frac{m_e}{m_0} - (\frac{m_e}{m_0})^2} \tag{1.1}$$

where c is the speed of the light and $\gamma = \frac{1}{\sqrt{1-\beta^2}}$

Charged particles are characterized by a definite range in the given absorber material. The range represents a distance beyond which no particles will penetrate. The products of these encounters in the absorber are either excited atoms or ion-pairs. Each ion-pair is made up of a free electron and the corresponding positive ion of an absorber atom from which an electron has been totally removed. The ion pairs have a natural tendency to recombine to form neutral atoms, but in some detectors, this recombination is suppressed so that the ion pairs may be used as the basis of the detector response.

1.1.1 Stopping power

During the passage of a particle through a medium with the atomic number Z and atomic mass A the mean energy loss energy loss per unit length(linear stopping power) of the charged particle (except electrons and positrons) is defined as follows :

$$S = -\frac{dE}{dx} \tag{1.2}$$

The classical expression [7] that describes the specific energy loss is known as the *Bethe formula* and is written as :

$$-\frac{dE}{dx} = K z^2 \frac{Z}{A} \frac{1}{\beta^2} \left[\frac{1}{2} log \frac{2m_e c^2 \beta^2 \gamma^2 T_{max}}{I^2} - \beta^2 - \frac{C}{Z} - \frac{\delta}{2} \right] \tag{1.3}$$

where $K = 4\pi N_A {r_e}^2 m_e c^2$.

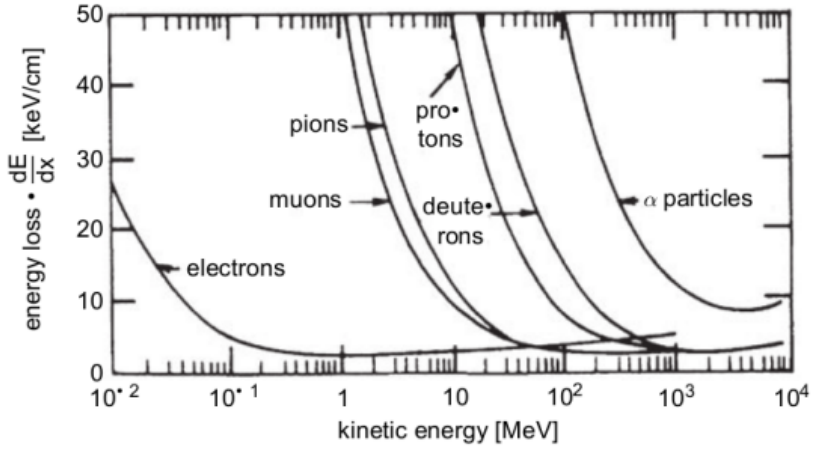

Figure 1.1: Variation of the specific energy loss in air versus energy of the charged particle. For energies above a few hundred MeV all particles have the same energy loss.

In this expression, N_A, r_e, I and δ denote respectively Avogadro's number, classical electron radius, mean excitation potential which is $10.2eV$ and the density effect correction. The C/Z is the "shell correction" term, which becomes important at the lowest energies for particles having energy comparable to the energy of electrons bound in the medium. For non-relativistic charged particles ($v << c$), only the first term of the Eq.1.3 is significant. Since $log\left(\frac{2m_ec^2\beta^2\gamma^2T_{max}}{I^2}\right)$ is a slowly varying function, hence stopping power is nearly inversely proportional to the energy. Hence, we can conclude following things from the above formula

- Charged particle spends a greater time when its velocity is low, the impulse felt by the electron, and the energy transfer, is largest.
- When comparing different charged particles with the same velocity, particles with the greatest charge will have the largest specific energy loss.
- When comparing absorber materials, the one with the high atomic number and high-density will result in greatest linear stopping power.

The variation of the specific energy loss for a number of different charged particles is shown in Fig.1.1 over a wide energy range. The figure depicts that the value of dE/dx for different types of charged particles approaches a near-constant broad minimum value at energies above several hundred MeV, where their velocity approaches the velocity of light. The specific energy loss corresponds to about 2 MeV per g/cm^2 in

light materials. Because of their similar energy loss behavior, such relativistic articles are called "minimum ionizing particles". The energy loss increases again for $\gamma > 4$ (logarithmic rise or relativistic rise) because of the logarithmic term in the bracket of Eq.1.3. The increase follows approximately a dependence like $2ln\gamma$.A large fraction of the logarithmic rise relates to large energy transfers to few electrons in the medium (δ rays or knock-on electrons). Because of the density effect, the logarithmic rise of the energy loss saturates at high energies.

The Bethe formula begins to fail at low particle energies where charge exchange between the particle and absorber becomes important. Low energy electrons and positrons loose energy due to both ionization and other processes such as Moller and Bhabha scattering and photon emission. This occurs when they are decelerated in the Coulomb field of a nucleus (bremsstrahlung) which starts to dominate above a few tens of MeV. In case of electrons, the maximum energy T_{max} transferred in a single collision is reduced to :

$$T_{max} = E - m_e c^2 \tag{1.4}$$

Assuming that the incident electron energy is greater than the electron binding energy medium atoms, energy loss is mainly due to multiple collisions resulting in ionization and excitation of the medium atoms, given by the following expression [8].

$$\left(-\frac{dE}{dx}\right)_c = \frac{2\pi N Z e^4}{\beta^2 m_e c^2} log[\frac{(\gamma-1)\beta^2 E^2}{2I^2}] + \frac{1}{\gamma^2}[\frac{(\gamma^2 - 2\gamma + 9)}{8} - (2\gamma - 1)log2] \tag{1.5}$$

while the fraction of energy loss due to bremsstrahlung is described by:

$$\left(-\frac{dE}{dx}\right)_{rad} = \frac{4\pi N E \alpha Z(Z+1)e^4}{{m_e}^2 c^4}[log(2\frac{E}{m_e c^2}) - \frac{1}{3}] \tag{1.6}$$

where α, E and e denote the fine-structure constant, electron enrgy and charge respectively. The total energy loss by electron is given by the sum :

$$\left(-\frac{dE}{dx}\right)_{tot} = \left(-\frac{dE}{dx}\right)_c + \left(-\frac{dE}{dx}\right)_{rad}. \tag{1.7}$$

1.1.2 Energy loss characteristics

1. **THE BRAGG CURVE**

   A plot of the specific energy loss along the track of a charged particle is known as a *Bragg curve*. The energy loss of a heavy ion is characteristically different from

that of an electron. The ion picks up negative charges in the form of electrons on its path through the detector medium. The more the velocity of the ion, the less is the probability of it interacting with the medium and consequently it deposits less energy in the detector. However as it penetrates more into the medium, its energy decreases and it starts interacting effectively with the detector atoms. This is what is responsible for the gradual increase in the energy deposited in the absorber medium with distance penetrated. Once the average velocity of the ion reduces to almost zero, it deposits its maximum energy at one go and this is what corresponds to the Bragg Peak, which plays an important role in the proton radiation therapy. By means of this, the proton beam energy can be tuned in such a way, that a uniform dose of energy with a good localization can be delivered to the volume of interest. The ion having deposited all its energy has no more energy available to interact and hence the stopping power drops sharply following this peak.

2. **ENERGY STRAGGLING**

   The sharpness of the Bragg Peak is decreased in the practical scenario. The reason for this is the statistical nature of the incidence of the heavy ions. Two identical ions may interact with the medium in an entirely different way. Hence even the range of any two such ions will be different. This amounts to a finite spread around the Bragg Peak.

   The stochastic nature of the ion-medium interaction implies that even a mono-energetic beam will pick up a finite spread in its energy after penetration. This spread keeps on increasing till the Bragg Peak is reached as the rate of energy loss increases with distance. Finally, after the ion beam has deposited almost all of its energy, the energy distribution narrows again. This phenomenon is known as energy straggling.

1.1.3 Interaction of gamma rays

Gamma rays interact with matter via three dominant processes- photoelectric absorption, Compton scattering and pair production.

Photoelectric absorption

The gamma ray photon interacts with an absorber atom in which it is completely absorbed ejecting an energetic photoelectron from one of its bound shells. Most

energetic gamma rays eject the photoelectron from the tightly bound K shell of the atom. The energy of the photoelectron is given by

$$E_e = h\nu - E_b \tag{1.8}$$

where E_e is the energy of the ejected electron, E_b is the binding energy of the photoelectron in its original shell and $h\nu$ is the energy of the incident gamma ray photon. Following the photoelectric absorption characteristic X-ray photons may also be generated. The vacancy left by the ejected photoelectron is quickly filled by the capture of a free electron or the rearrangement of electrons from the outer shells of the atom which in turn emits one or more characteristic X-ray photons. X-ray emission may also occur from the less tightly bound L or M shells. The excited atom may even lose its excess energy by the emission of Augur electrons that give rise to a discrete spectrum.

The photoelectric effect is a predominant mechanism for energy loss of gamma rays of relatively low energy.It also dominates when the absorber material has higher atomic number. The probability of photoelectric absorption per atom (τ) is related to the incident gamma ray energy and the absorber atomic number by

$$\tau \sim \frac{Z^n}{{E_\gamma}^{3.5}} \tag{1.9}$$

where the exponent n varies from 4 to 5. In the low energy region, discontinuities in the curve or absorption edges appear at gamma ray energies corresponding to the binding energies of electrons in the shells of the absorber atom. The edge with highest energy corresponds to the bonding energy of the K-shell electron and the subsequently lower energy edges represent those of L, M and other shells.

Compton scattering

The interaction via Compton scattering takes place between an incident gamma ray photon and a free electron in the absorber material. The photon gets deflected through an angle θ with the original direction and transfers its energy partially to the electron which gets scattered off in a different direction as a recoil electron. The final energy of the scattered photon is related to its incident energy and the angle of deflection by

$$h\nu^{'} = \frac{h\nu}{1 + \frac{h\nu}{m_0 c^2}(1 - \cos\theta)} \tag{1.10}$$

where m_0c^2 is the rest mass energy of the electron and $h\nu$ and $h\nu^{'}$ are the initial and final energies of the photon. We find that the energy loss is very little for small scattering angles and maximum energy transfer occurs for angles close to π. The probability of Compton scattering per atom (σ) depends on the number of electrons available as scattering targets and thus linearly increases with Z, i.e.

$$\sigma \sim Z \tag{1.11}$$

The probability generally falls off gradually with gamma ray energy. The amount of energy transferred to the electron in a single scattering is given by

$$\Delta E = h\nu \frac{\frac{h\nu}{m_0c^2}(1-\cos\theta)}{1+\frac{h\nu}{m_0c^2}(1-\cos\theta)} \tag{1.12}$$

The maximum energy transferred to the electron in a single scattering is

$$\Delta E_{max} = h\nu \frac{\frac{2h\nu}{m_0c^2}}{1+\frac{2h\nu}{m_0c^2}} \tag{1.13}$$

which occurs at angle of scattering equal to π. This value of energy transferred is referred to as Compton Edge. We see that even at the maximum angle of scattering the gamma ray photon retains a part of its energy.

Pair production

Pair production is a possible process of energy loss in the absorber medium if the gamma ray energy exceeds twice the rest mass energy of an electron (1.02 MeV). When the incident energy rises to several MeV range, a single gamma ray photon may disappear and be replaced by an electron-positron pair. The excess energy is transformed into kinetic energy shared by the electron and the positron respectively. The positron however subsequently undergoes an annihilation on encounter with an electron and two annihilation photons are emitted. The probability for pair production per nucleus (κ) approximately varies as the square of the absorber atomic number (Z), i.e.

$$\kappa \sim Z^2 \tag{1.14}$$

1.1.4 Gas Ionization by Fast Charged Particles

A charged particle that traverses the gas in a drift chamber leaves a track of ionization along its trajectory. The encounters with the gas atoms are purely random and are characterized by a mean free flight path λ between ionizing encounters given by the ionization cross-section per electron σ_{I} and the density N of electrons:

$$\lambda = \frac{1}{N\sigma_I} \tag{1.15}$$

Therefore, the number of encounters along any length L has a mean of L/λ, and the frequency distribution is the Poisson distribution.

$$P(L/\lambda, K) = \frac{(L/\lambda)^K}{K!} \exp(-L/\lambda) \tag{1.16}$$

If a gas counter with sensitive length L is set up so that the presence of even a single electron in L will always give a signal, then its inefficiency may be identified, thus measuring λ.

1.2 Different Ionization Mechanisms

For the detection of particles, what we have to know in the first place is the amount of ionization along the track and the associated fluctuation phenomena. The average energy loss by ionization and excitation can be transformed into a number of electron-ion pairs produced along the track of a charged particle. There are basically two types of ionization mechanisms:

- Primary Ionization
- Secondary Ionization

One must distinguish between primary ionization, that is the number of primarily produced electron-ion pairs, and the total ionization. A sufficiently large amount of energy can be transferred to some primarily produced electrons so that they also can ionize. This secondary ionization together with the primary ionization forms the total ionization.

1.2.1 Average energy required to produce one ion-pair

Only some part of the energy lost by the fast particle is spent in ionization. The total amount of ionization from all processes is characterized by the energy W, that is spent on average on the creation of one free electron.

The amount of ionization produced by particles that lose all their energy in the gas is measured by ionization chambers or proportional counters.

- For pure noble gases, W varies between 46 eV for He and 22 eV for Xe.
- For pure organic vapors, the range is between 23 to 30 eV.

1.2.2 The Range of Primary electrons

Primary electrons are emitted almost perpendicular to the track as their momentum remains very small compared to the one of the track. They lose their kinetic energy in collisions with the gas molecules, scattering almost randomly and producing secondary electrons, until they have lost their kinetic energy.

In argon at N.T.P., an electron of 1 keV is stopped in about $30\mu m$, and one of 10 keV in about 1.5 mm. Only 0.05% of the collisions between the particle and the gas molecules produce primary electrons with kinetic energy larger than 10 keV.

1.3 The Drift of Electrons and Ions in Gases

The behavior of the drift chamber is crucially dependent on the drift of the electrons and ions that are created in the avalanches at the electrodes.

Therefore it is important to understand how the drift velocity vector in electric and magnetic fields depends on the properties of the gas molecules, including their density and temperature.

1.3.1 An Equation of Motion with Friction

The motion of charged particles under the influence of electric and magnetic fields, E and B may be understood in terms of an equation [1] of motion:

$$m\frac{du}{dt} = e\vec{E} + e[\vec{u} \times \vec{B}] - ku \tag{1.17}$$

where $\tau = \frac{m}{k}$

The solution for $t >> \tau$ of eq.(1.17) is a steady state for which $\frac{du}{dt} = 0$. Hence, the equation becomes :

$$\frac{u}{\tau} - \frac{e}{m}[\vec{u} \times \vec{B}] = \frac{e}{m}\vec{E} \tag{1.18}$$

Let $(e/m)B_x = \omega_x$ and $(e/m)E_x = \varepsilon_x$ and and expressing (1.18) in the form of the matrix equation :

$$Mu = \varepsilon,$$
$$M = \begin{bmatrix} \frac{1}{\tau} & -\omega_z & \omega_y \\ \omega_z & \frac{1}{\tau} & -\omega_x \\ -\omega_y & \omega_x & \frac{1}{\tau} \end{bmatrix} \tag{1.19}$$

The solution is obtained by inverting M:

$$u = M^{-1}\varepsilon$$
$$M^{-1} = \begin{bmatrix} 1+\omega_x^2\tau^2 & \omega_z\tau + \omega_x\omega_y\tau^2 & -\omega_y\tau + \omega_x\omega_z\tau^2 \\ -\omega_z\tau + \omega_x\omega_y\tau^2 & 1+\omega_y^2\tau^2 & \omega_x\tau + \omega_y\omega_z\tau^2 \\ \omega_y\tau + \omega_x\omega_z\tau^2 & -\omega_x\tau + \omega_y\omega_z\tau^2 & 1+\omega_z^2\tau^2 \end{bmatrix} \frac{\tau}{1+\omega^2\tau^2} \tag{1.20}$$

where $\omega^2 = \omega_x^2 + \omega_y^2 + \omega_z^2 = (e/m)^2B^2$. The compact form of writing :

$$\vec{u} = \frac{\tau e}{m}|\vec{E}|\frac{1}{1++\omega^2\tau^2}\left(\hat{E} + \omega\tau(\hat{E} \times \hat{B}) + \omega^2\tau^2(\hat{E}.\hat{B})\hat{B}\right) \tag{1.21}$$

The drift direction is governed by the dimensionless parameter $\omega\tau$, where ω is defined as $(e/m)|B|$ and carries the sign of the charge of the moving particle. When $\vec{E}$ is parallel to $\vec{B}$ (i.e. $\omega\tau = 0$) then :

$$\vec{u} = \frac{\tau e}{m}|\vec{E}| = \mu\vec{E} \tag{1.22}$$

and the electron velocity is not affected by the presence of a magnetic field and is the same as in its absence. In case of $\vec{E}$ perpendicular to $\vec{B}$:

$$\vec{u} = \frac{\tau e}{m}|\vec{E}|\frac{1}{1+\omega^2\tau^2}\left[\begin{bmatrix}1\\0\\0\end{bmatrix} - \omega\tau\begin{bmatrix}0\\1\\0\end{bmatrix}\right] \tag{1.23}$$

It leads to the deviation of the electron trajectory as compared to that of in absence of magnetic field by an angle which is equal to $arc\tan\frac{u_y}{u_x} = arc\tan(-\omega\tau)$.

On the microscopic scale, the electrons and ions that drift are scattered on by the gas molecules in a random direction. On average, they assume a constant drift velocity **u** in the direction of the electric field **E** (or, if a magnetic field is also present, in the direction which is given by both fields).

1.4 Microscopic Picture

In the microscopic picture of electron motion in gases [1], an electron due to its low mass scatters randomly. In addition, it has an instantaneous velocity **c** which in the presence of the external electric field immediately increases up to **u** which is introduced in the macroscopic model and defined by eq.(1.22). In a drift distance x with n collisions $n = \frac{x}{u\tau}$. If λ denotes the average fractional energy loss per collision, the energy balance is the following:

$$\frac{x}{u\tau}\lambda\varepsilon_E = eEx \tag{1.24}$$

Here the equilibrium energy ε_E carries an index E because it does not contain the part due to the thermal motion of the gas molecules, but only the part taken out of the electric field.

We have the average time between collisions same as the average time that has elapsed since the last collision. This is because in a completely random series of encounters, characterized only by the average rate $1/\tau$, the differential probability $f(t)dt$ that the next encounter is a time between t and $t + dt$ away from any given point $t = 0$ in time is :

$$f(t)dt = \frac{1}{\tau}e^{\frac{t}{\tau}}dt \tag{1.25}$$

Independent of the point where the time measurement begins. In the frictional- motion picture, τ was the ratio of the mass of the drifting particle over the coefficient of friction. In the microscopic picture, τ is the mean time between the collisions of the drifting particle with the atoms of the gas. For drifting particles with instantaneous velocity c, the mean time τ between collisions may be expressed in terms of the cross-section σ and the number density N :

$$\frac{1}{\tau} = N\sigma c \tag{1.26}$$

Here c is related to the total energy of the drifting electron by;

$$\frac{1}{2}mc^2 = \varepsilon = \varepsilon_E + \frac{3}{2}kT \tag{1.27}$$

For electron drift in particle detectors, we usually have $\varepsilon_E >> (3/2)kT$, we can neglect the thermal motion, and (1.22), (1.24), and (1.27) combine to give the two equilibrium velocities as follows:

$$u^2 = \frac{eE}{mN\sigma}\sqrt{\frac{\lambda}{2}}, \tag{1.28}$$

$$c^2 = \frac{eE}{mN\sigma}\sqrt{\frac{2}{\lambda}}, \tag{1.29}$$

where $\varepsilon = (1/2)mc^2 \approx \varepsilon_E = (3/2)kT$.

Chapter 2

Properties of Gas Mixtures

2.1 Introduction

The knowledge of the drift and diffusion properties of electrons and ions in gases is of primordial importance for the understanding of the operational characteristics of proportional gaseous detectors and to improve their performances. For this reason, considerable study has been made in this thesis on a large number of gases, both individual and mixtures, invariably in order to optimize counter operation for particle detection, identification, and localization. The results obtained from conventional gas mixtures used for particle detection are compared with that of using air as the gas mixture.

For tracking at the high luminosity hadron collider like LHC, an operational gas mixture [15] has the following requisites: It has to be fast so that an event can be unambiguously associated to its bunch crossing which leads to a compromise between having a high drift velocity and large primary ionization statistics. The most commonly used filling gas is 90% Ar + 10% CH_4 mixture designated as P-10. The drift velocity would ideally be saturated or have a small variation with modifications in electric and magnetic fields. The mixture needs to be well quenched with no secondary effects like photon feedback and field emission giving a stable gas gain well separated from the noise of the electronics.

2.2 Electron Transport Properties

The rigorous mathematical theory that lays the foundation for electron transport has already been discussed in the previous chapter. In the absence of electric field, the

free electrons in the gas will move randomly experiencing collisions with gas molecules with a Maxwell energy [15] distribution, having an average thermal energy of 3/2 kT(0.04 eV at STP). When an electric field is applied, in addition to the random thermal velocity, the electrons begin to drift in the direction of the field with a mean velocity v_d (the average distance covered by the electron per unit time). The energy distribution in the absence of electric field becomes even more complicated once the electrons start moving in the electric field and thus acquiring energy. The momentum transfer per collision is not a constant, especially in excitation and ionization collisions between electrons and atoms, causing a larger energy loss. Electrons with energies near the Ramsauer minimum in argon 2.1 for example (0.23 eV) have long mean free paths and as a consequence can gain more energy before experiencing a collision with the surrounding gas. The drift velocity is also dependent on pressure, temperature and can be modified by the presence of pollutants like water or oxygen.

Differently from noble gases, poly-atomic molecular and organic gases have many other modes of dissipating energy, namely molecular vibrations and rotations. The probabilities of these mechanical excitations can be as important as those of electronic excitations. The actual mechanism of such interactions is complex and the molecule can be in a final state very different from the ground state of the molecule. The cross sections of carbon-dioxide can be taken as an example Fig.2.3. It is seen that these collisions are produced at relatively small energies (0.1 to 1 eV) compared to ionization and excitation collisions.

2.2.1 Diffusion and Drift

As the electrons are drifting in the electric field they also disperse symmetrically thus giving rise to volume diffusion, transverse and longitudinal to the direction of motion. In cold gases like carbon-dioxide for example, the diffusion is small, while drift velocity is low and unsaturated for values of electric field usual in gas detectors. This implies a nonlinear space-time relation. Warm gases like argon have a higher diffusion. When mixed with polyatomic/organic gases having vibrational thresholds between 0.1 and 0.5 eV, diffusion is reduced in most cases, while the drift velocity is increased.

In the absence of an external field the electrons and ions move uniformly away from the point of creation which is referred to as the diffusion. The electron diffusion along any given direction $\vec{x}$ is related to the velocity $\vec{v}$ and follows a Gaussian distribution

Table 2.1: Properties of noble and molecular gases at normal temperature and pressure (NTP: $20°C$, one atm). E_X , E_I : first excitation, ionization energy;W_I : average energy per ion pair; $dE/dx|_{mip}$,N_P , N_T : differential energy loss, primary and total number of electron-ion pairs per cm, for unit charge minimum ionizing particles.

Gas	Z	A	Density	E_X	E_I	W_I	$dE/dx\|_{mip}$	N_P	N_T	Radiation Length
			$mgcm^{-3}$	eV	eV	eV	$keVcm^{-1}$	cm^{-1}	cm^{-1}	m
He	2	2	0.178	19.8	24.5	41	0.32	4.2	8	745
Ar	18	39.9	1.782	11.6	15.7	26	2.44	23	94	110
Ne	10	20.2	0.90	16.7	21.56	36.3	1.56	12	43	345
Xe	54	131.3	5.86	8.4	12.1	22	6.76	44	307	15
CF_4	42	88	3.93	12.5	15.9	54	7	51	100	92.4
DME	26	46	2.2	6.4	10.0	23.9	3.9	55	160	222
CO_2	22	44	1.98	5.2	13.7	33	3.01	35.5	91	183
CH_4	10	16	0.71	9.8	15.2	28	1.48	25	53	646
C_2H_6	18	30	1.34	8.7	11.7	27	1.15	41	111	340
$i-C_4H_{10}$	34	58	2.59	6.5	10.6	23	5.93	84	195	169

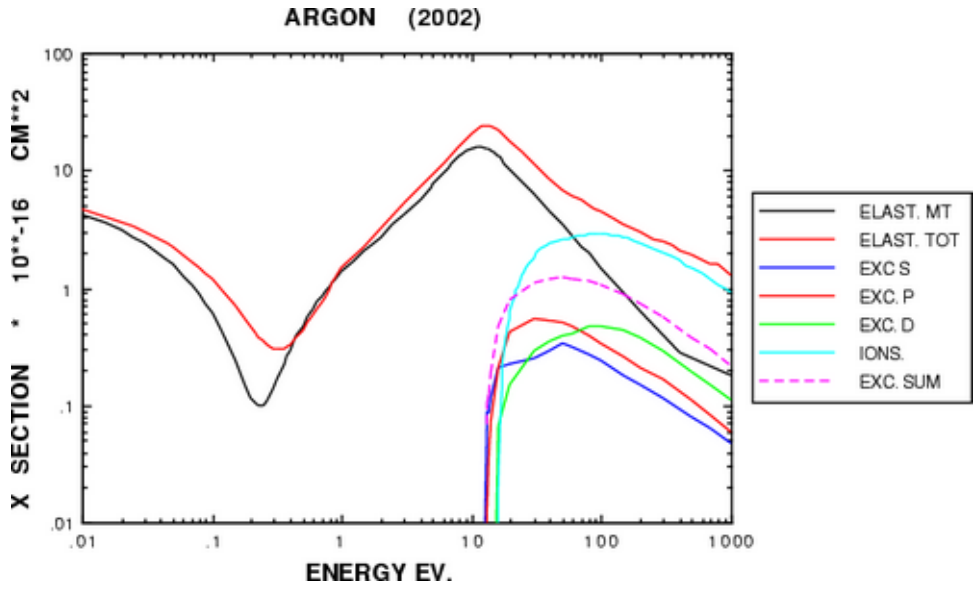

Figure 2.1: Cross-sections for electron collisions in Argon as a function of their energy [4], [5]

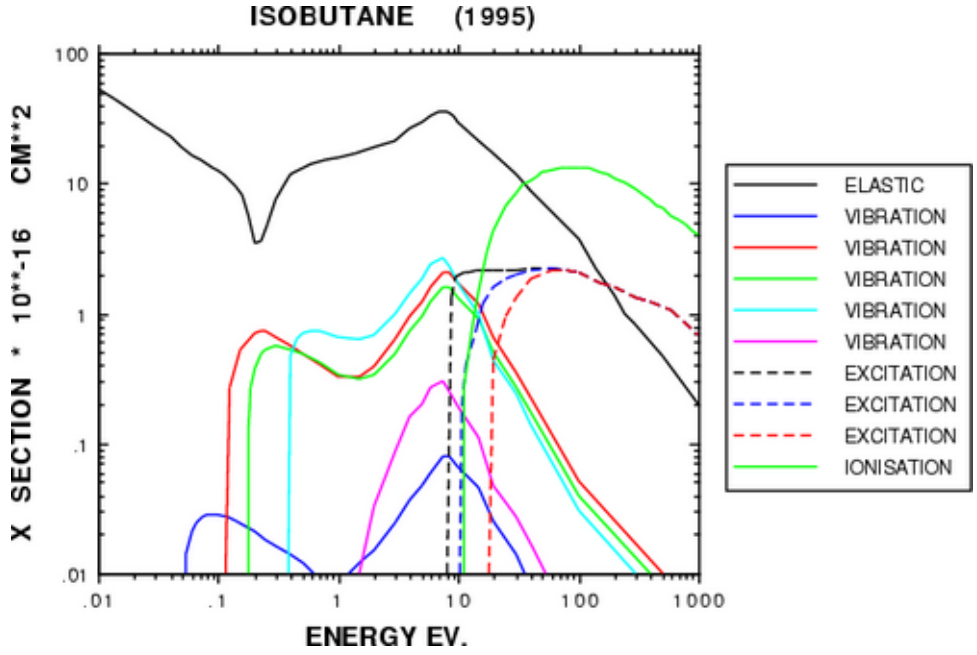

Figure 2.2: Cross-sections for electron collisions in Isobutane [4], [5]

with the following standard deviation [17]

$$\sigma_x = \sqrt{\frac{2Dx}{u}} \tag{2.1}$$

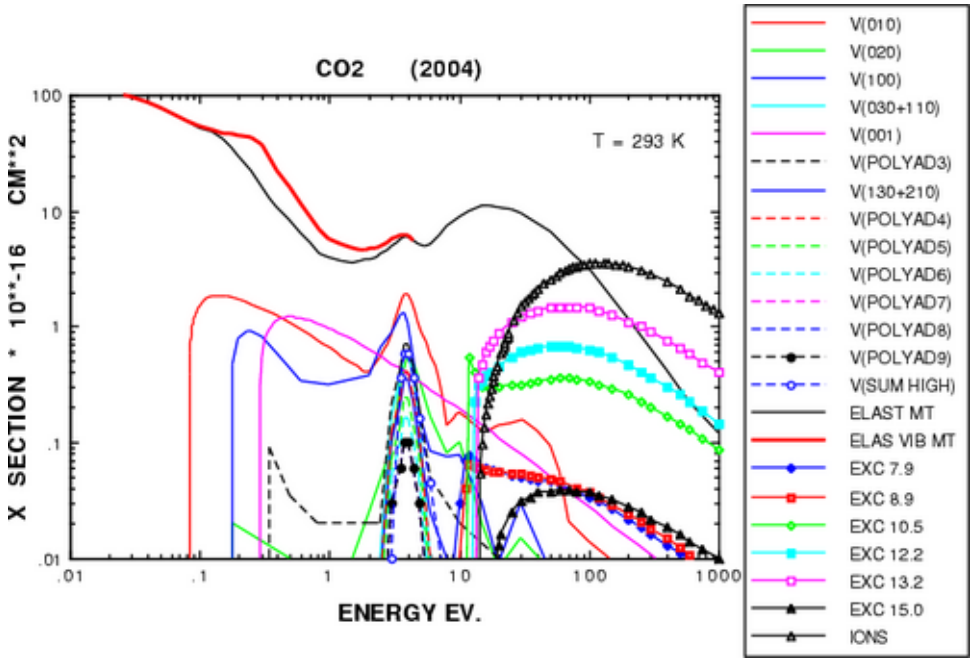

Figure 2.3: Cross-sections for electron collisions in carbon-dioxide calculated using Magboltz [4], [5]

where D is a field dependent diffusion coefficient which is determined by the average free path length λ of e^- and ions in the gas:

$$D = \frac{1}{3} v_{diff} \lambda \tag{2.2}$$

where v_{diff} is the average diffusion velocity. In the ideal case, where electrons do not modify their energy at increasing values of E, the mean collision time τ is constant, the drift velocity increases linearly with the field, and the following relationship holds:

$$eE\frac{D}{u} = kT \tag{2.3}$$

from which and Eq.2.8 the expression for σ_x can be obtained:

$$\sigma_x = \sqrt{\frac{2kTx}{eE}} \tag{2.4}$$

referring to the thermal limit to electron diffusion. In the description of diffusion, a characteristic energy ε_k is introduced

The dependence of electron drift velocity on the electric field varies with the type of gas used.

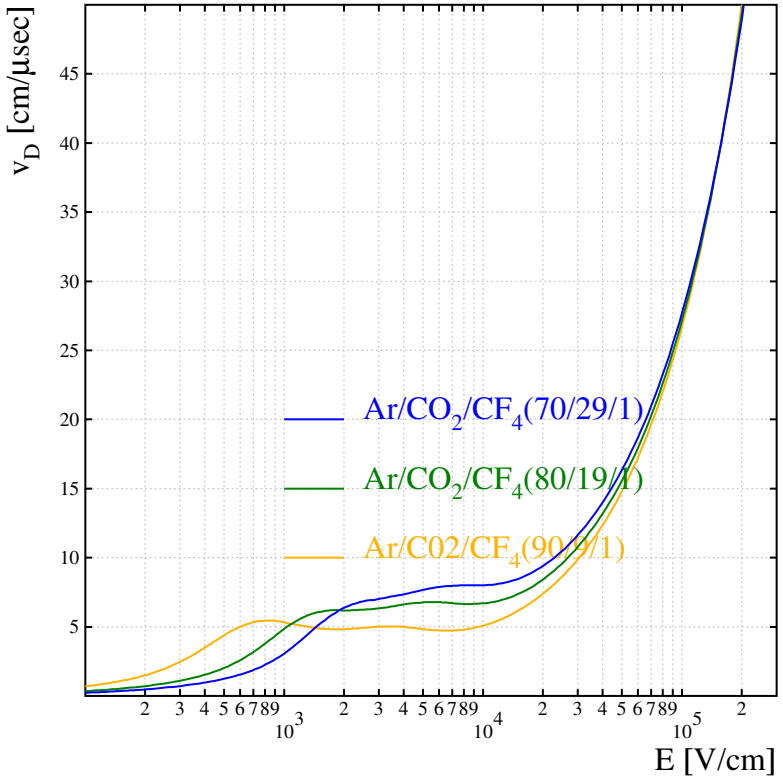

Figure 2.4: Electron drift velocity calculated with Magboltz for $\mathrm{Ar}/CO_2/CF_4$ gas mixture

2.2.2 Amplification

Townsend Coefficient

The average distance an electron travels between ionizing collisions is called mean free path and its inverse is the number of ionizing collision per cm α which is defined as the first Townsend coefficient. The first Townsend coefficient α depends on the field strength $\vec{E}$ and thereby on the position x in the gas counter. This parameter helps in determining the gas gain of the gas. If N_0 is the number of primary electron without amplification in the uniform electric field and N is the number of electrons after distance x under avalanche condition. Then N is given by:

$$N(x) = N_0 e^{\int \alpha(x) dx} \tag{2.5}$$

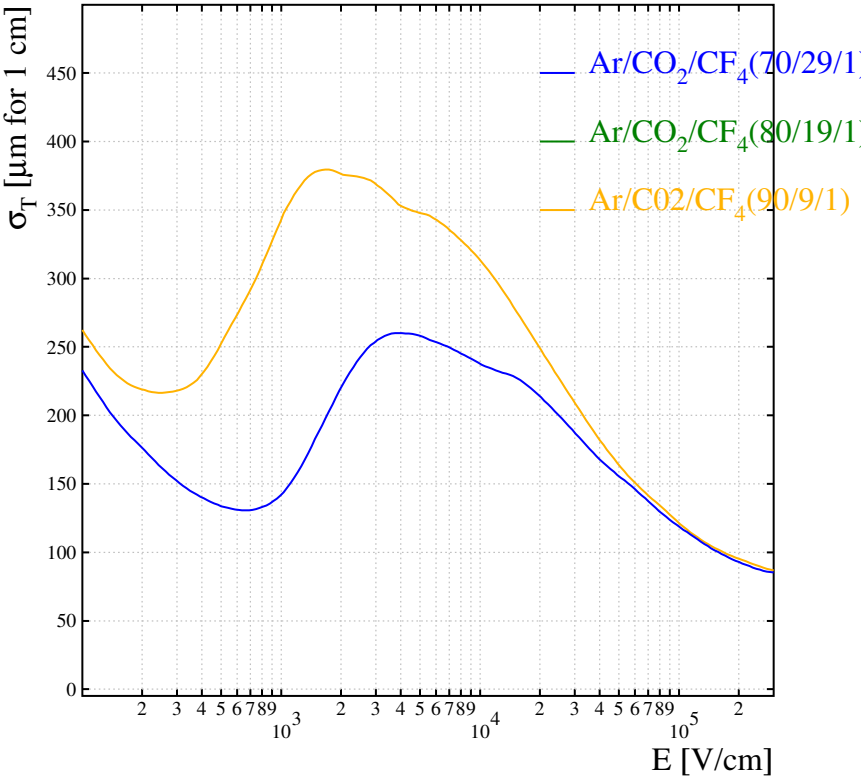

Figure 2.5: Transverse diffusion coefficient calculated with Magboltz for $Ar/CO_2/CF_4$ gas mixture

where the gas amplification factor is given by :

$$A = exp \int_{r_k}^{r_i} \alpha(x) dx \tag{2.6}$$

The lower integration limit is fixed by the distance r_k from the center of the gas counter, where the electric field strength exceeds the critical value E_k from which point on charge-carrier multiplication starts. The upper integration limit is the anode-wire radius r_i. The proportional range of a counter is characterized by the fact that the gas amplification factor A takes a constant value. As a consequence, the measured signal is proportional to the produced ionization. Gas amplification factors of upto 10^6 are possible in the proportional mode. Typical gas amplifications are rather in the range between 10^4 upto 10^5. The integration of the current at the output of the

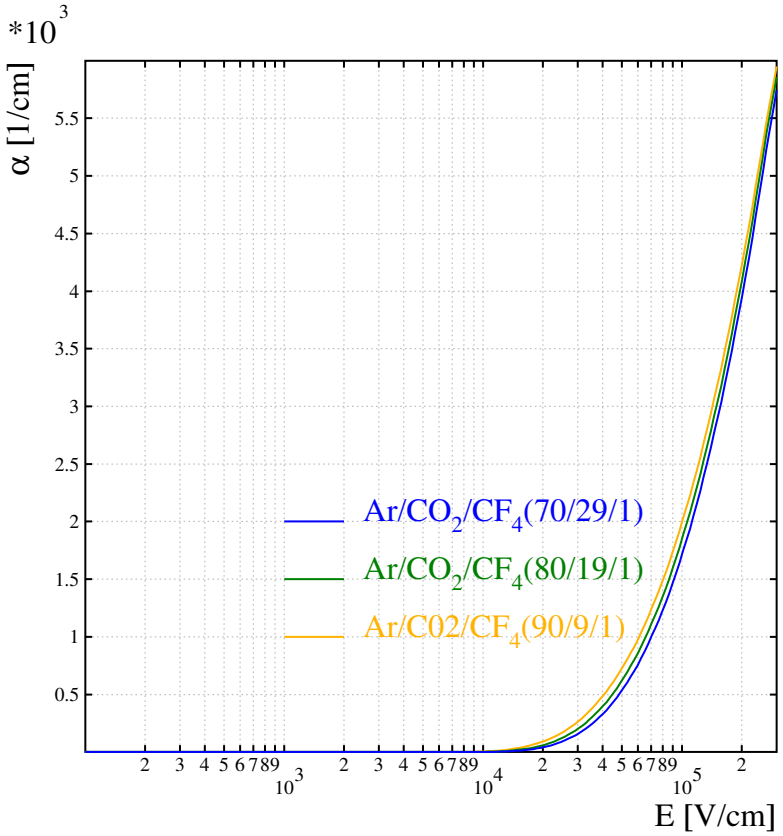

Figure 2.6: Townsend Coefficient as a function of the electric field for $\mathrm{Ar}/CO_2/CF_4$ gas mixture

proportional counter leads to the gas-amplified charge :

$$Q = \int i(t)dt \tag{2.7}$$

which is again given by the relation $Q = e.N_0A$. From the current integral and the known primary ionization N_0 the gas amplification A can be easily obtained.

Penning effect

The Penning effect occurs in gas mixtures, in which a metastable excited state of one gas component is energetically higher than the ionization energy of the second gas component. The excited gas atoms/molecules ionize the second gas through collisions and hence increase of the number of electron-ion pairs. Penning gas mixtures consist typically of a noble gas (in most cases Ar) and a low concentration admixture of a molecular gas.

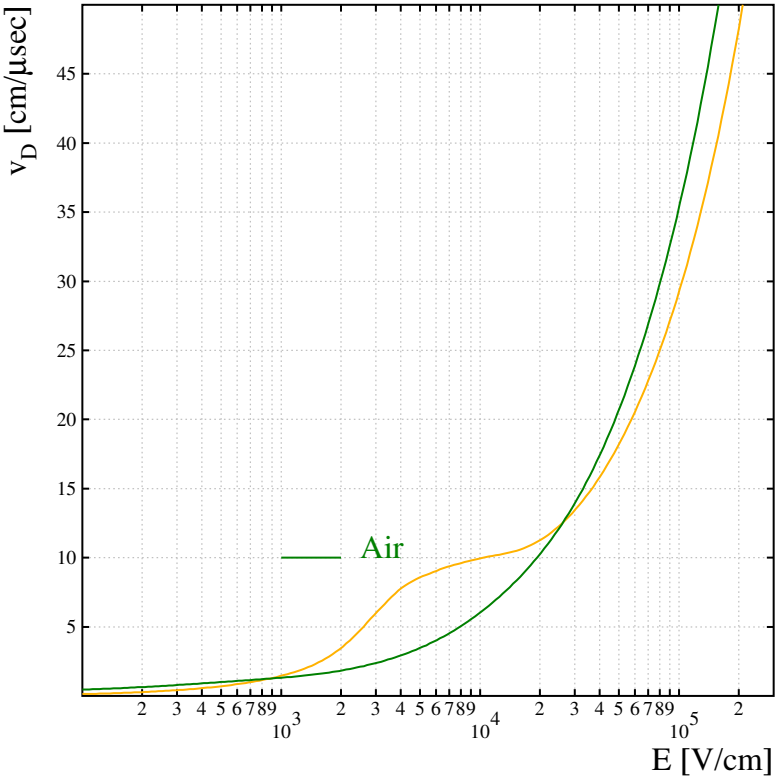

Figure 2.7: Electron drift velocity calculated with Magboltz for CF_4/CO_2/Ar (10:50:40) mixture(Yellow) and Air(Green) as the gas mixture

2.3 Ion Transport Properties

Ions drift slowly due to their large mass and scattering cross-section. The ion mobility is defined as the ratio of drift velocity v_i of the ions and the reduced electric field (E/p), in the absence of magnetic field, where E and p are the electric field and pressure respectively. It is almost constant up to rather high fields being specific to a particular ion moving in a specific gas.

During the passage of ions in the gas, they encounter collisions with the gas molecules loosing energy such that up to the high strength of electric fields their energy remains thermal. In low electric fields the ion drift velocity is proportional to $\vec{E}$ while ion mobility μ ($\vec{u} = \mu\vec{E}$) is independent of $\vec{E}$:

$$u = \sqrt{\frac{M+m}{Mm}}\sqrt{\frac{1}{3kT}}\frac{eE}{N\sigma} \tag{2.8}$$

where m and M denote ion and gas molecule mass, respectively.

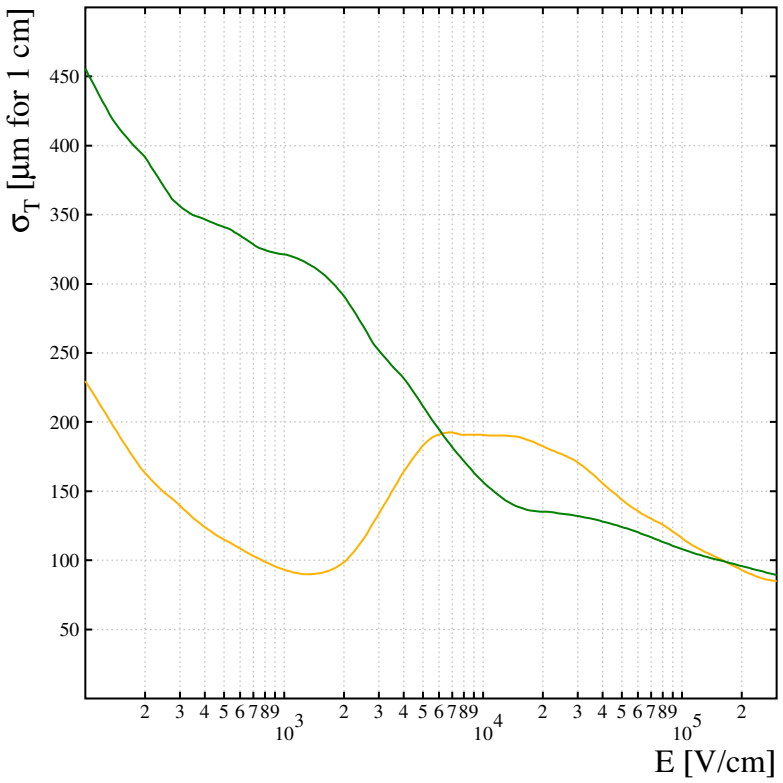

Figure 2.8: Transverse diffusion coefficient calculated with Magboltz for CF_4/CO_2/Ar (10:50:40) mixture(Yellow) and Air(Green) gas mixture

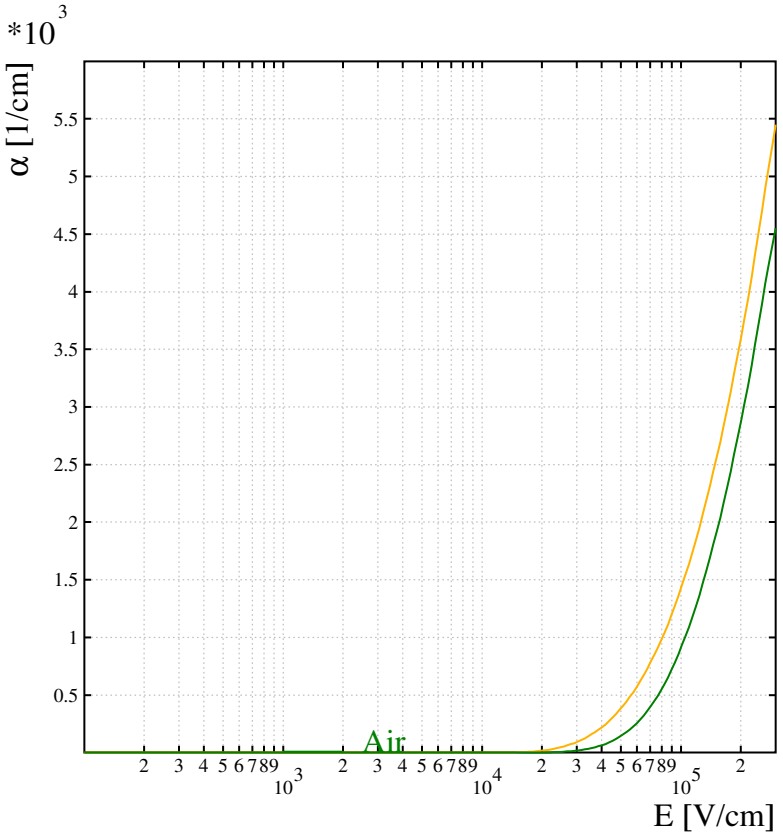

Figure 2.9: Townsend Coefficient as a function of the electric field for gas mixtures: CF_4/CO_2/Ar (10:50:40)(Yellow) and Air(green) calculated with Magboltz program

Chapter 3

Computer Programs for Gas Detector Simulation

3.1 Heed

Heed [3] is a computer program written by Igor Smirnov that computes in detail the ionization energy loss of fast charged particles in gases, taking delta electrons and optionally multi-scattering of the incoming particle into account. By means of the Monte Carlo calculation, the energy transfers from the incident particle to the atomic electrons can be simulated. After knocking out of a primary delta-electron a vacancy will remain in the atomic shell. The number of shells with vacancies and the type of atoms in the gas mixture is specified for every energy transfer. The program can generate individual events for further processing by a user program, but can also compute such quantities as :

- No. of clusters per cm;
- Cluster size distribution;
- Range and straggling of delta electrons

3.2 Magboltz

Magboltz [5] is a simulation program of electron motions in gases under the influence of uniform electric and magnetic fields. It computes electron drift velocity, the longitudinal and transverse diffusion coefficients, the Townsend and attachment coefficients

as well as the excitation and ionization rates for the various gas molecules. The calculations are based on the Monte-Carlo technique introduced by Sakai [19] and Itoh [20]. The method of an electron tracking between two parallel plates can be outlined as follows: the electron motion path is approximated to be series of linear segments with a length equal to 0.1 of the mean free path which corresponds to electron energy. At the end of each segment, the decision of collision occurrence between electron and gas molecules is taken with a random number generator. If the electron is judged to collide, the kind of collision will be determined according to electron energy. The cross-sections as a function of energy for different electron-gas molecules collisions for argon, carbon dioxide and isobutane are presented in Fig.2.1, 2.2, 2.3. After the collision, the electron energy is reduced by an adequate amount. The new direction of electron motion was decided according to a random number generator.

3.3 neBEM (nearly exact boundary element method)

The nearly exact boundary element method (neBEM) [24] solver has been developed [21],[22] recently and used successfully to solve difficult problems related to electrostatics [23]. The study of the electrostatic field plays a key role in optimizing the detector geometry so as to get a desired configuration for the field in a given volume as per the tracking requirement. A novel formulation of the BEM, the nearly exact BEM (neBEM) solver was developed to resolve some of the major drawbacks of usual BEM. The neBEM uses exact integration of the Greens function and its derivative in its formulation.

3.4 Garfield

The entire simulation of the proposed detector has been done using Garfield. Garfield is a drift chamber simulation program by R.Veenhof [4]. It simulates charge drift in a detector, calculates the gas gain and the charge or electric current induced on the read-out electrodes. By means of this program, the spatial and timing resolution of the chamber can also be estimated. Garfield has an interface to the Magboltz [5] program which computes electron transport properties in nearly arbitrary gas mixtures. Garfield also has an interface with the Heed [3] program to simulate ionization of gas molecules by particles traversing the chamber. Garfield is interfaced with the

neBEM [24] program as well. However, some assumptions are made in the simulation performed with Garfield :

- The electric field established in the chamber is static;
- The presence of charges does not influence either the electric field or other free charges.
- The photoelectrons from the electrodes and photons released during the gas-molecules de-excitation processes are not taken into consideration.

The program can calculate for instance the following:

- Field maps, contour plots, and 3-dimensional impressions;
- The wire sag that results from electrostatic and gravitational forces;
- Optimum potential settings to achieve various conditions;
- Plots of electron and ion drift lines;
- x(t)-relations, drift time tables and arrival time distributions;
- Signals induced by charged particles traversing a chamber, taking both electron pulse and ion tail into account.

Chapter 4

Multiwire Proportional Chambers

4.1 Introduction

The invention of the Multi-wire Proportional Chamber (MWPC) by G.Charpak in the 1960s heralded the era of "electronic detectors" in high energy particle physics, an achievement for which he was awarded the Nobel Prize for Physics in 1992.

An MWPC is based on a set of parallel thin anode wires closely spaced, all at the same potential, each wire acting as an independent counter, symmetrically sandwiched between two cathode planes. Fig.4.3 gives a schematic of the cross-section of the structure. For proper operation, the gap length D is three or four times larger than the wire spacing d. When a negative potential is applied to the cathodes, the anode being grounded an electric field develops as indicated by equipotentials and field lines in Fig.4.1 and in a magnified view around the anodes in Fig.4.2 [12]. When an ionizing particle passes through the gas volume thus creating electron-ion pairs, the electrons will drift along the field lines until they approach the high field region where avalanche multiplication occurs.

Close to the wires, the field strength increases so as to initiate a Townsend-avalanche: electrons become energetic enough to ionize the gas and in turn grow exponentially in numbers. The gas which is used as the ionizing medium usually consists of $60 - 90\%$ noble gas, mostly argon, whereas additional molecular gas needs to be mixed such as CO_2 or methane to ensure stable avalanche formation. To obtain fast signals, gases with high electron mobility are used. MWPCs are sensitive to all forms of ionizing radiation. High energy charged particles ionize the gas with typically 100 electrons liberated along the path of 1cm length, which in turn are amplified on the anode wires.

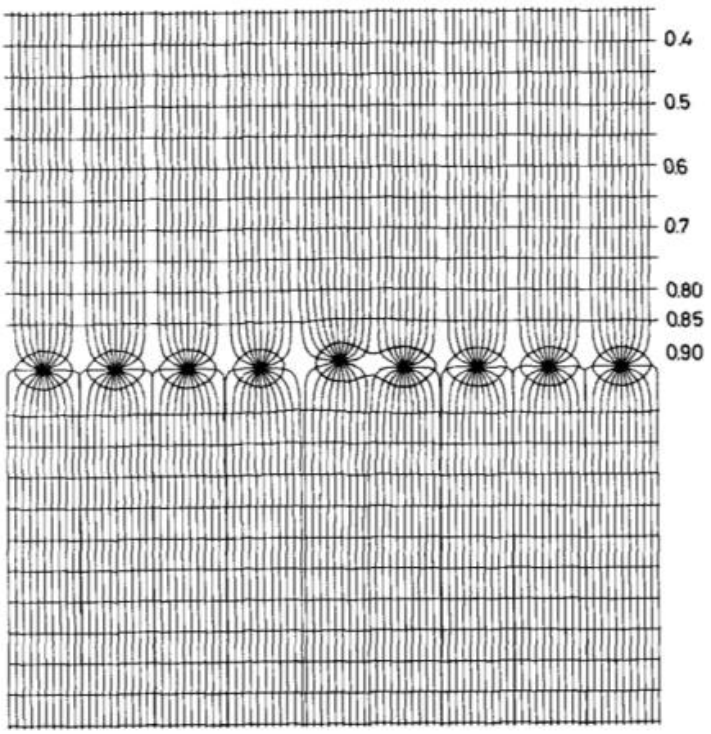

Figure 4.1: Electric field equipotentials and drift lines in MWPC. The effect on the field of a small displacement of one wire is also shown [12],[26]. When a the symmetric potential difference is applied between anodes and cathodes, an electric field develops perpendicular to the anodes.Two main regions of the field, leading to the particular behavior of the counter, can be identified: a) A region of roughly constant field extending in most of the gap, b) A region of a rapidly increasing field around the wires where avalanche multiplication occurs. Moreover, low field regions exist between the wires with some consequences on the collection properties of the chamber.

The wires in an MWPC are special in the sense that they must be thin enough to produce the sufficiently high electric field close to the surface, and at the same time need to be strong enough to ensure mechanical stability. The detectors with the very large surface area can be constructed economically by placing a grid of anode wires between two large flat plates that serve as cathodes on either side.

When the coordinates of the wires are $y = 0, x = 0, \pm d, \pm 2d, ...$ the potential distribution is approximated by an analytical form [26]:

$$V(x,y) = \frac{CV}{4\pi\epsilon_0}\{\frac{2\pi D}{d} - ln\left[4\left(sin^2\frac{\pi x}{d} + sinh^2\frac{\pi y}{d}\right)\right]\} \tag{4.1}$$

$$E(x,y) = \frac{CV_0}{2\epsilon_0 d}\left(1 + tan^2\frac{\pi x}{d}tanh^2\frac{\pi y}{d}\right)^{1/2}\left(tan^2\frac{\pi x}{d} + tanh^2\frac{\pi y}{d}\right)^{-1/2} \tag{4.2}$$

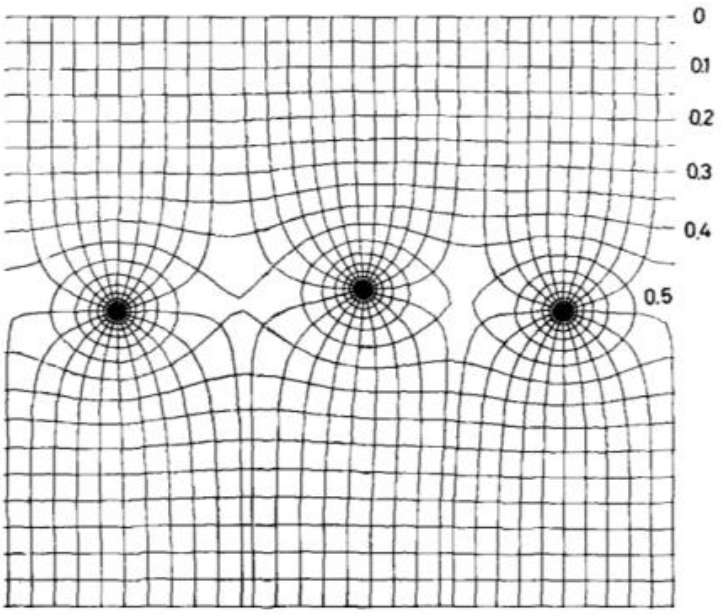

Figure 4.2: Enlarged view of the field around the anode wires(wire spacing 2mm and wire diameter 20μm [26]

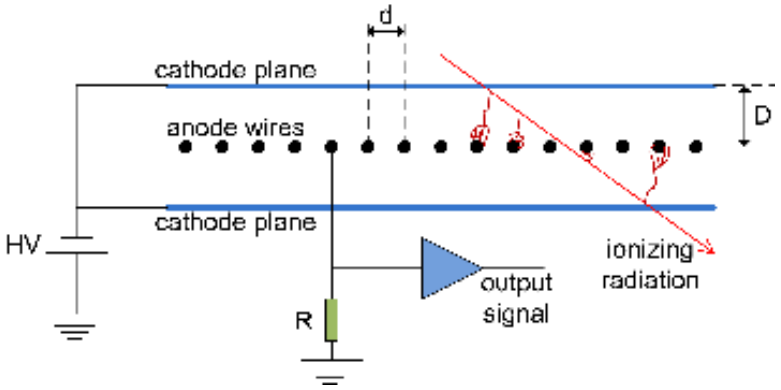

Figure 4.3: Schematic diagram of a MWPC read out

where D and d are defined in Fig.4.3, V is the anode voltage, ϵ_0 the permittivity of free space and C the capacitance per unit length given by the formula:

$$C = \frac{4\pi\epsilon_0}{2\left(\frac{\pi D}{d} - ln\frac{2\pi r_i}{d}\right)} \tag{4.3}$$

where r_i is the anode-wire radius.

Along the symmetry lines x = 0, y = 0, the elctric field can be written as:

$$E_y = E(0, y) = \frac{CV_0}{2\epsilon_0 d} coth\frac{\pi y}{d} \tag{4.4}$$

$$E_x = E(x,0) = \frac{CV_0}{2\epsilon_0 d} cot \frac{\pi x}{d} \tag{4.5}$$

It is instructive to consider the following approximations:

$$For \quad y << d; \quad E(x,y) = \frac{CV_0}{2\pi\epsilon_0} \frac{1}{r} \tag{4.6}$$

where $r = \sqrt{x^2 + y^2}$.

$$for \quad y \geq s \quad coth \frac{\pi y}{d} \approx 1, E_y = \frac{CV_0}{2\epsilon_0 d} \tag{4.7}$$

Eq.4.6 shows that the field is radial around the wire, with an expression identical to that of the cylindrical proportional counter.

4.2 Operational Characteristics of MWPC

4.2.1 Principle of Operation

There are six regions of operation which can be distinguished by the characteristic of the avalanche size as a function of the voltage as follows:

At zero voltage, no charge is collected as the ion-electron pairs recombine due to an electrical attraction. As the voltage is increased, the recombination forces are overcome and the current begins to increase as more and more of the electron-ion pairs are collected before they can recombine. At some point, all created pairs will be collected and a further increase in voltage shows no effect. This corresponds to the first flat region in fig. (4.4). A detector working in this region (II) is called an *ionization chamber* since it collects ionization produced directly by the passing radiation. If we now increase the voltage beyond region II we find that the current increases again with the voltage. At this point, the electric field is strong enough to accelerate freed electrons to an energy where they are also capable of ionizing gas molecules in the cylinder. The electrons emitted in these secondary ionizations then accelerate to produce still more ionization and so on. This results in an ionization *avalanche*. The ensuing avalanche multiplication provides a large gain, a factor as large as 10^5 or more. A schematic view of the avalanche process is found in Fig. 4.5. The number of electron-ion pairs in the avalanche is directly proportional to the number of primary electrons. This region of proportional multiplication extends upto point III and a detector operating in this domain is known as *proportional chamber*. If the voltage

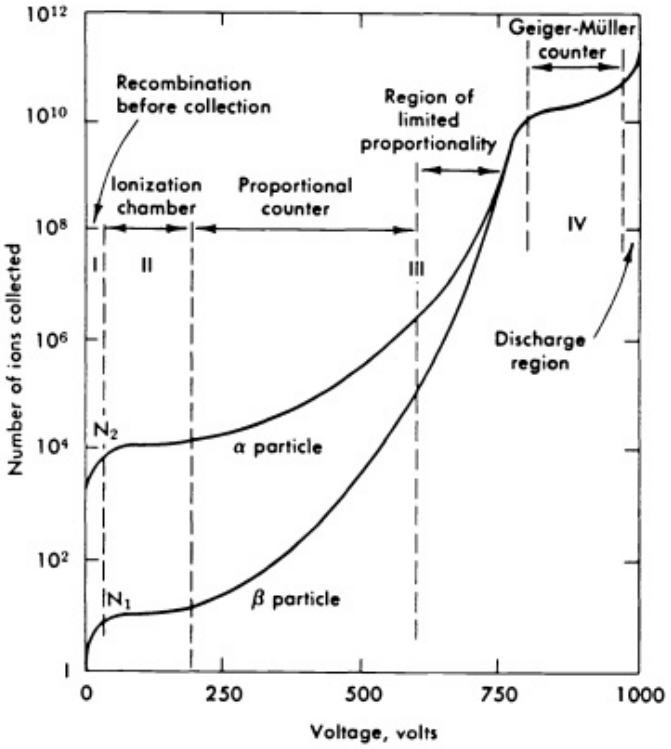

Figure 4.4: Gain Voltage Characteristics for a proportional Counter showing the different regions of operation

is now increased beyond point III, the total amount of ionization created through multiplication becomes sufficiently large that the space charge created distorts the electric field about the anode. Proportionality thus begins to be lost. This is known as the region of limited proportionality. Increasing V still higher, the energy becomes so large that a discharge occurs in the gas. What physically happens is that instead of a single localized avalanche at some point along the wire, a *chain reaction* of many avalanches are caused by photons emitted by de-exciting molecules which travel to other parts of the counter to cause further ionizing events. The output current thus becomes completely saturated, always giving the same amplitude regardless of the energy of the initial event. Detectors working in this voltage region are called *Geiger-Muller* counters. The Geiger voltage region is characterized by a plateau over which the count rate varies little. Finally, if the voltage is increased still further a continuous breakdown occurs with or without radiation. This region is to be avoided to prevent damage to the counter. We thus see how phenomena such as gas multiplication and discharge, in addition to gas ionization can be used for radiation detection.

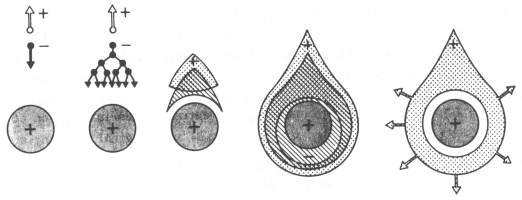

Figure 4.5: Time development of an avalanche in a proportional counter. A single primary electron proceeds towards the anode, in regions of increasingly high fields, experiencing ionizing collisions; due to the lateral diffusion, a drop-like avalanche, surrounding the wire, develops. Electrons are collected during a very short time (1 ns or so) and a cloud of positive ions is left, slowly migrating towards the cathode.

4.2.2 Chamber Parameters

The accuracy of localization in the multi-wire proportional chamber is determined by the anode wire-spacing, however, a spacing of less than 2 mm is increasingly difficult to operate. Decreasing the wire pitch results in improved time resolution since the drift time is shorter and arrival time fluctuations are reduced. For a fixed wire diameter to obtain a given gain one has to keep the charge per unit length CV_0 constant, that increases V_0 when wire spacing is decreased. For e.g. going from 2 mm to 1 mm spacing V_0 has to be almost doubled. At the same time, however electric field in the drift region is also doubled. The chance that some drifting electrons meet the Raether limit (physical limiting value of the multiplication factor (M) or gas gain in an ionization avalanche process) is strongly increased. Practically 1 mm wire spacing is difficult to operate on surfaces larger than 100 cm^2 or so. Decreasing the wire diameter helps but there are obvious mechanical and electrostatic limitations. Scaling down all geometrical parameters (i.e. distance and diameters of the wires, gas gap) is not sufficient to preserve good operation, in fact the mean free path for ionization remains invariant unless the gas pressure is increased.

4.2.3 Choice of Gas

A general discussion on properties of gas mixtures for gas detectors was given in chapter 3. The filling gas in MWPC should be chosen from those species that do not show an appreciable electron attachment coefficient because gas multiplication is critically dependent on the migration of free electrons rather than much slower negative ions. A stable proportional or semi-proportional operation can be achieved

in mixtures of argon or xenon with carbon dioxide, methane, isobutane, ethylene, ethane etc. A typical gain of 10^5 can be obtained before breakdown.

Air is sometimes used as a proportional gas for alpha counting. Air could not serve as a proportional gas for beta detection, because beta particles produce far fewer ion pairs in the gas than alphas. Since more electrons travel towards the anode following an alpha interaction in the gas, there is a greater chance that some of them will avoid interacting with oxygen and produce an avalanche. Also, if the detector is designed so that the electrons dont have far to travel to the anode, there is less chance that they will interact with the oxygen. Using air as the proportional gas allows the use of a thin window without the need for a gas flow system. However, it is essential that the air be dry. In high humidity conditions, air proportional counters are prone to generating spurious pulses.

4.2.4 Factors governing the proportional amplification

The factors affecting the proportional amplification in MWPC are as follows:

- The amplification of a proportional counter increases exponentially with the applied voltage above a threshold V_0. But as the voltage is raised one finds that: firstly the strict proportionality between deposited ionization and signal is lost and secondly, further increase in voltage lead to sparking.

- Decreasing the gap length decreases the total voltage required, however the ionization deposited by a minimum ionizing particle will also decrease, while the capacitance has increased, so we need a higher amplification.

4.2.5 Time development of the signal

There are two contributions to the effective rise-time of a pulse. First one is the time it takes to collect the electrons liberated in the gas, the second is the motion of the ions away from the central wire 4.17d.

MWPCs are typically operated with typical multiplications of 10^4 to 10^5 and the mean free path of electrons in the gas is much less than the typical wire radius, almost all the ion-pairs are formed very near to the wire. The whole process begins at a few wire radii typically at less than 50 μm from the anode surface. If the drift velocity of electrons in this region is 5 cm/μsec, it appears that the whole process of multiplication will take place in less than 1 nsec. At that instant electrons have been

collected at the anode and the positive ion sheath will drift towards the cathode at decreasing velocity. The detected signal, negative on the anode and positive on the cathode is the consequence of the change in the energy of the system due to movement of ions. Simple electrostatic considerations show that if a charge Q is moved by dr in a system of total capacitance (lC), where l is the length of the counter, the induced signal is:

$$dv = \frac{Q}{CV_0}\frac{dV}{dr}dr \tag{4.8}$$

Electrons in the avalanche are produced very close to the anode wire and their contribution to the pulse is very small since most of them travel through a small fraction of the total potential. It is the motion of the ions away from the central wire that induces the charge on the central wire. Assuming that all charges are produced at a distance λ from the wire, the elctron and ion contributions to the signal on anode will be:

$$V^- = -\frac{Q}{lCV_0}\int_a^{a+\lambda}\frac{dV}{dr}dr = -\frac{Q}{2\pi\epsilon_0 l}ln\frac{a+\lambda}{a} \tag{4.9}$$

$$V^+ = \frac{Q}{lCV_0}\int_{a+\lambda}^{b}\frac{dV}{dr}dr = -\frac{Q}{2\pi\epsilon_0 l}ln\frac{b}{a+\lambda} \tag{4.10}$$

The total maximum signal induced on the anode is:

$$V = V^+ + V^- = -\frac{Q}{2\pi\epsilon_0 l}ln\frac{b}{a} = -\frac{Q}{lC} \tag{4.11}$$

Substituting the typical values for a counter a = 10 μm, λ = 1 μm, b = 10mm, one finds that the electron signal contribution is about 1% of the total. It is therefore neglected for all practical purposes. The time development of the signal can easily be computed assuming the ions leaving the surface of the wire with constant mobility are the only contribution.

4.2.6 Induced Pulses

The proportional pulses in MWPCs are caused by the motion of positive ions away from the wire. This same motion induces signals of opposite polarity on neighboring wires. When the electrons from the primary ionizing event are all collected by one wire, that wire will produce a negative pulse, whereas the adjacent wires and the negative high voltage electrodes will have only positive pulses.

The amplitude of the induced positive pulses is proportional to that of the negative signal on the central wire. Typically the positive adjacent wire pulses are about 1/5

to 1/10 as large as the pulse on the central wire. The normal and the induced pulses are also completely correlated in time since it is the same motion of the same ions that are responsible for both the positive and the negative signals.

When the electrons from the primary ionization process are shared among several adjacent wires, for e.g. for an inclined track Fig.4.16c then one wire will receive electrons first, and the first avalanche will start there. This will induce positive signals on some of these neighbors. As the electrons from further out drift in they, in turn, will start avalanches on some of these neighbors, thus turning a pulse that originally started out positive into a negative one. In general, when there is a superposition of induced and normal pulses, it is the negative "normal" pulse which dominates.

4.2.7 Time resolution

The term time resolution is frequently used for the precision with which the arrival time of a particle in a detector can be recorded. The time resolution for individual events defined in this way is determined by the fluctuation of the rise time of the detector signal. In the operation of the chambers, several "times" are involved: the variable time delay between the passage of the particle and the arrival of the pulse at the logic system, the dead time, and the read-out time.

Maximum time jitter

Two principal factors are responsible for the delay time in MWPC: 1) The time it takes to collect the first few electrons produced when a particle ionizes the gas in the chamber; 2) The time it takes to amplify the pulse and to transmit it to the logic system. The time of arrival of the electrons in the amplifying region near the wire will depend on where in the chamber the primary ionization was produced. It will also depend upon the voltage applied to the electrodes, the gas mixture, the wire diameter and wire spacing and the energy loss of the particles traversing the chamber.

Time differences from adjacent wires

An ionizing particle produces pulses in several adjacent wires because the track may have been inclined with respect to the normal to the wire plane, δ-rays were produced, the electrons diffused laterally during the collection process, etc. When several adjacent wire share pulses, it is almost always the wire that produces the first pulse that is closest to the track. Often it is desirable to record only this first pulse and

to ignore the later arriving pulses from the other wires. By keeping the time window as short as possible one can minimize the number of events in which multiple pulses from adjacent wires are recorded.

Dead-Time

There is a minimum amount of time that must separate two events in order that they are recorded as two separate pulses. This minimum time separation is usually called the dead time.

The dead time of MWPCs is influenced by both internal and external factors. The internal limitations are due to the time it takes to collect all the electrons from the primary ionizing event, and also to a much lesser extent to the time it takes for the ion-avalanche to move away from the wire.

4.3 Simulation

4.3.1 Geometry of the Proposed Detector

We constructed a prototype chamber containing multiple wires to form layers or cells that function as independent proportional counters. This type of design provides multiple detector units that are in direct contact without intervening walls or dead layers. We tried various variations of the geometry 4.6 and finally fixed the geometry which gave the best results. For example Fig.4.8 illustrates an arrangement in which a center cell is surrounded by an annulus of cells, each made up of an anode wire at the center of a hexagonal array of wires that act as cell cathode. The main chamber parameters are listed in Table 1. We used a gas mixture of $CF_4/CO_2/Ar = 10/50/40$ to test our detector.

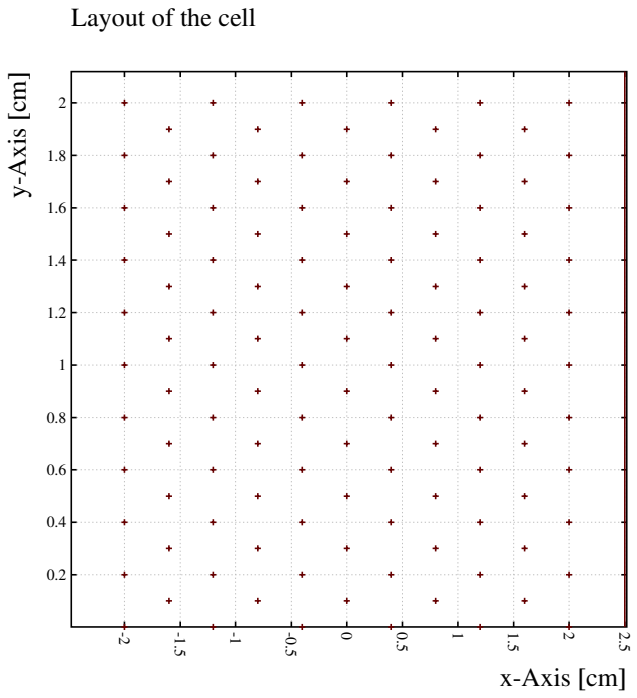

Figure 4.6: The cross sectional view of a multicell proportional counter. It consists of 11 set of wire planes.

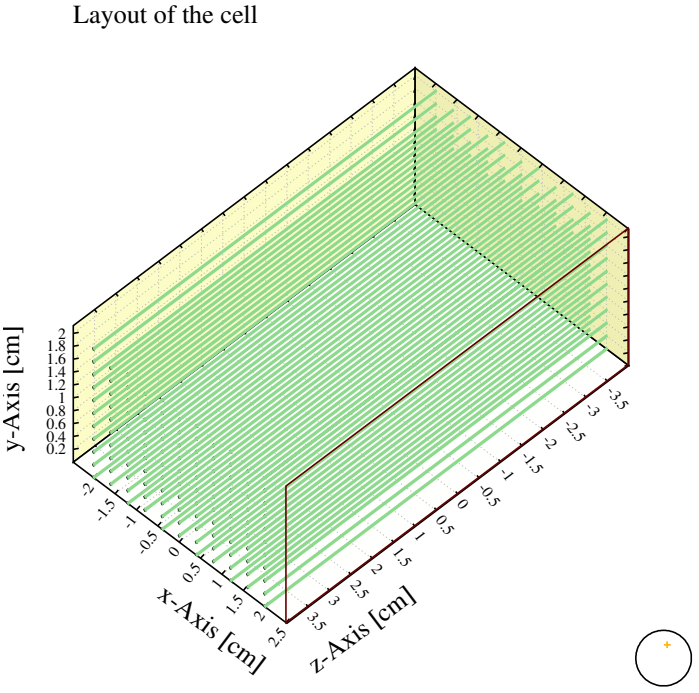

Figure 4.7: The 3-dimensional view of a multicell proportional counter.

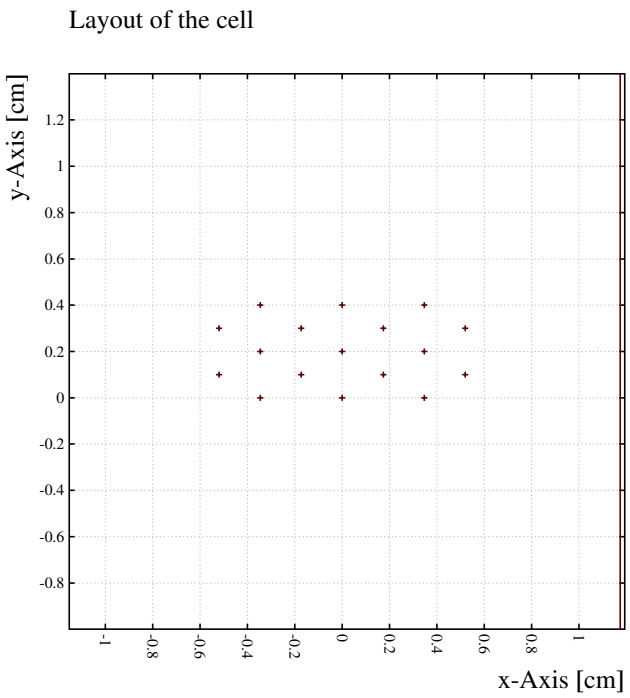

Figure 4.8: The cross sectional view of a multicell proportional counter. A single anode wire is at the center of each cell, surrounded by a grid of cathode wires.

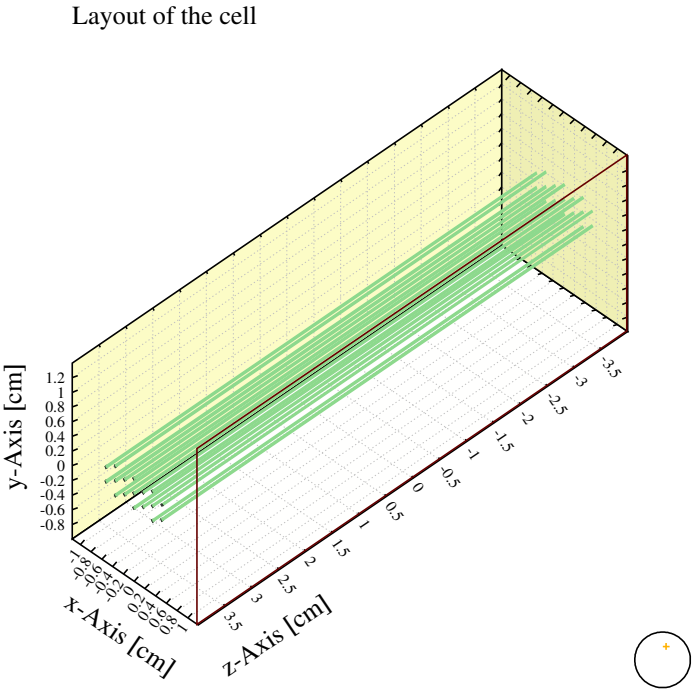

Figure 4.9: The 3-dimensional view of a multicell proportional counter. A single anode wire is at the center of each cell, surrounded by a grid of cathode wires.

Table 4.1: Main MWPC parameters

Gas gap thickness	24 mm
Wire spacing	1.732 mm
Wire diameter	250 μm
Wire Length	80 mm
Wire tension	0.7 N
Operating voltage	3500-4000 V
Gas mixture	Ar/CO_2/CF_4 40/50/10, Air

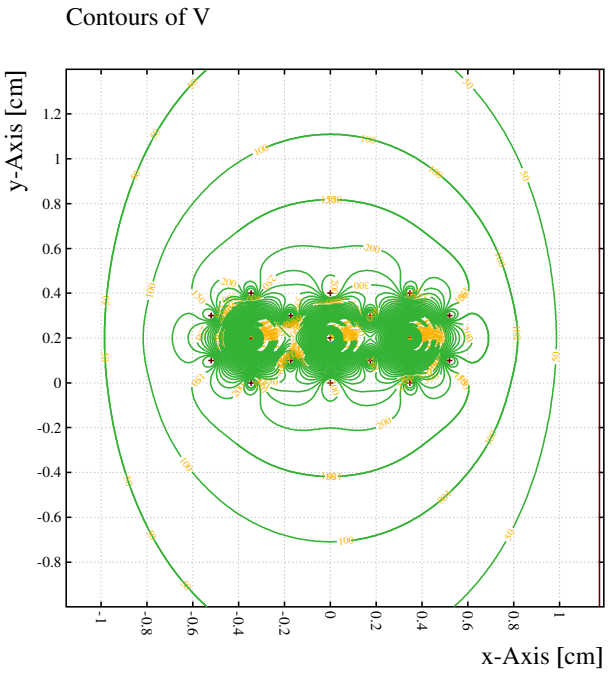

Figure 4.10: Equipotentials in a wire chamber. The distributions have been obtained by solving the Laplace Equations.

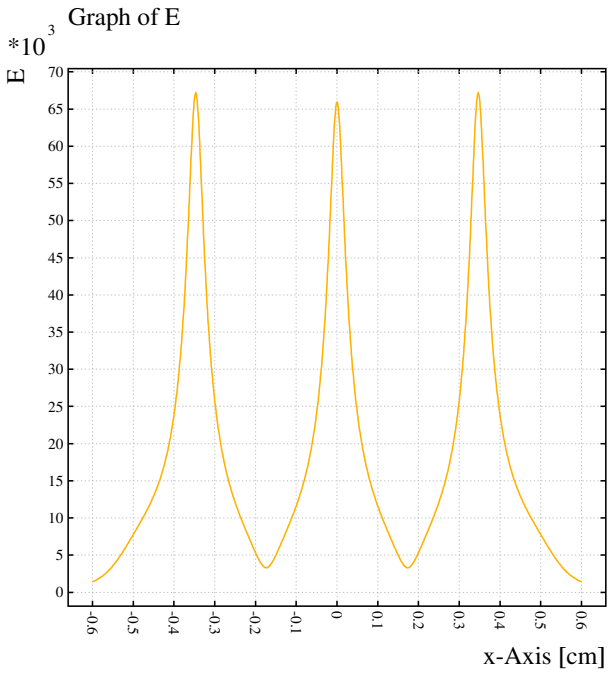

Figure 4.11: Electric field strength at the electrodes surface in MWPC. Voltage set on anode is 4000 V and 0 V at cathode. The maximum of the field is at the anode and it is high enough for an electron multiplication.

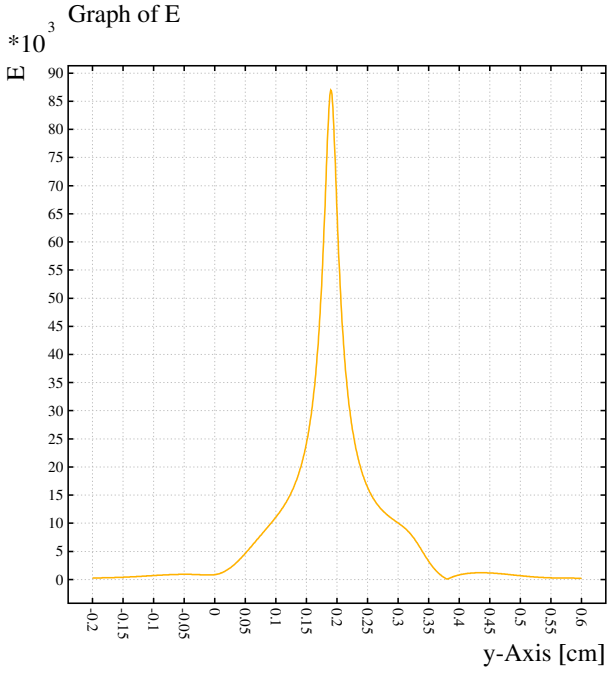

Figure 4.12: Electric field strength(in the y-axis) at the electrode as seen by the particle making 30 °angle with the x-axis.

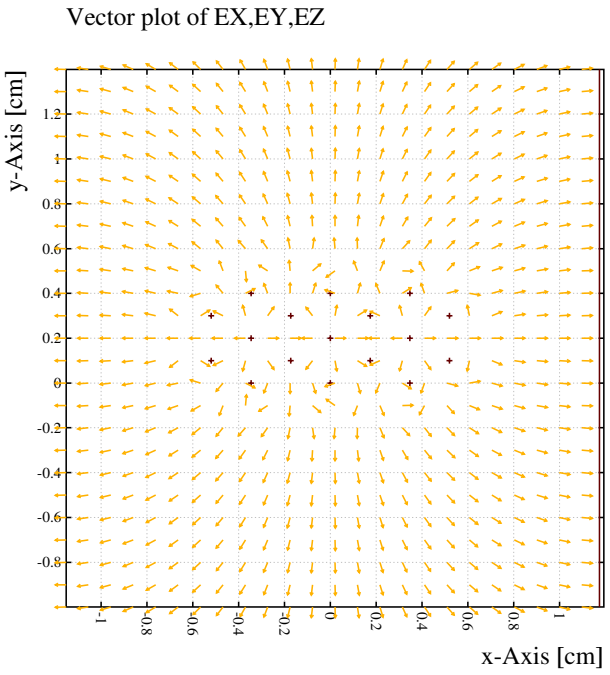

Figure 4.13: Vector plot for electric field

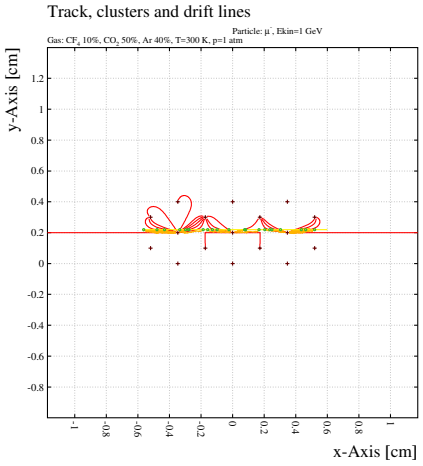

(a) Angle = 0°

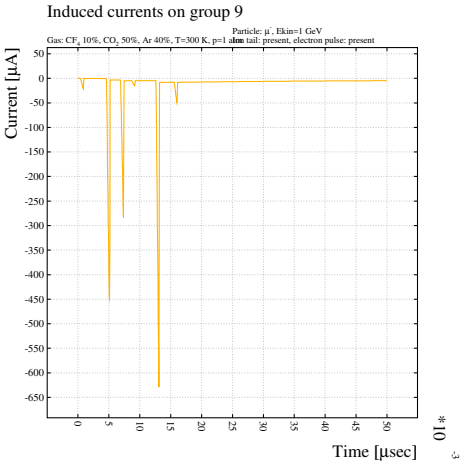

(b) Signal from wire-9

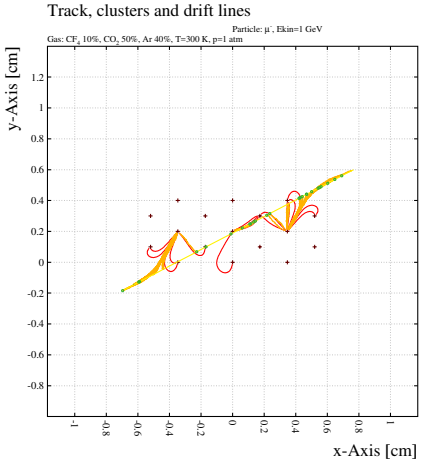

(c) Angle = 15°

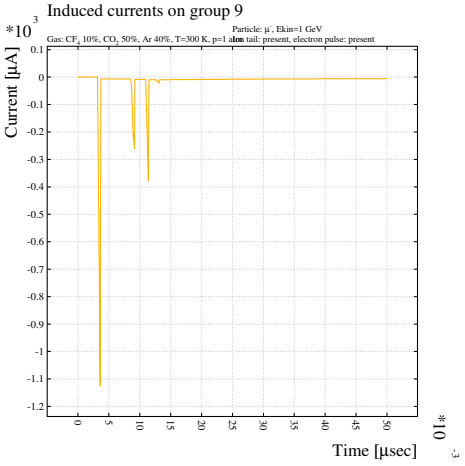

(d) Signal from wire-9

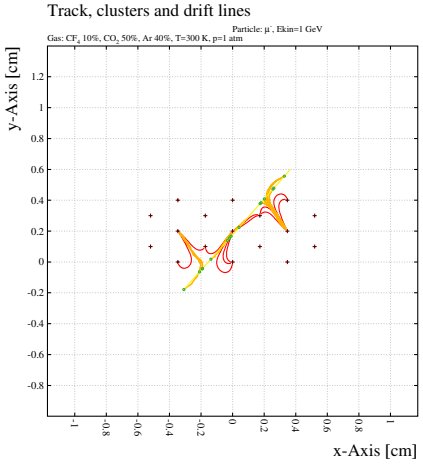

(e) Angle = 30°

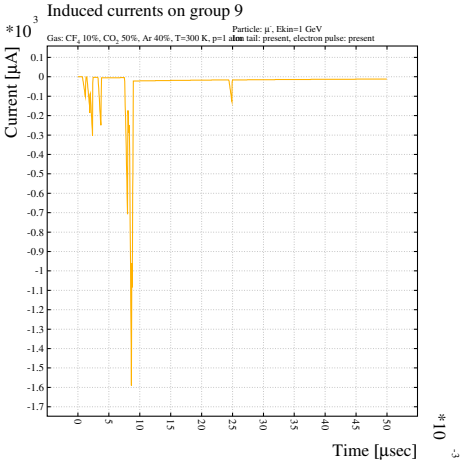

(f) Signal from wire-9

Figure 4.14: Track of the incoming muon of 1 GeV energy making various angle 0,15,30 to x-axis of the detector geometry and the corresponding signal induced by ion-movement on central anode wire at 4000 V for $Ar/CO_2/CF_4$ (40/50/10) as the gas mixture

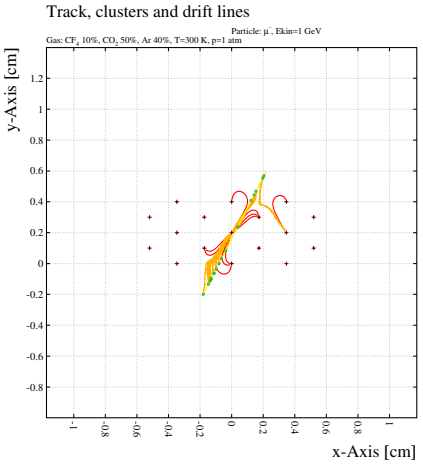

(a) Angle = 45°

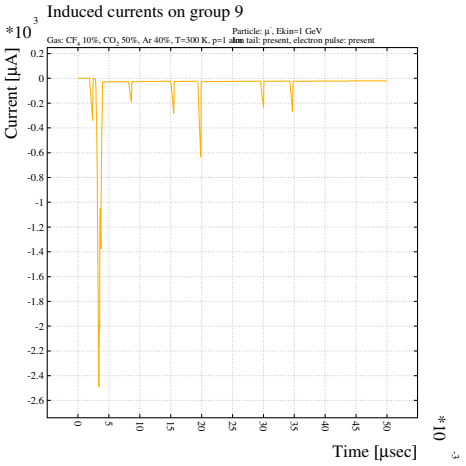

(b) Signal from wire-9

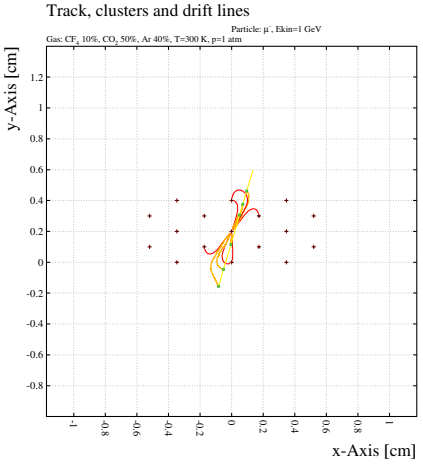

(c) Angle = 60°

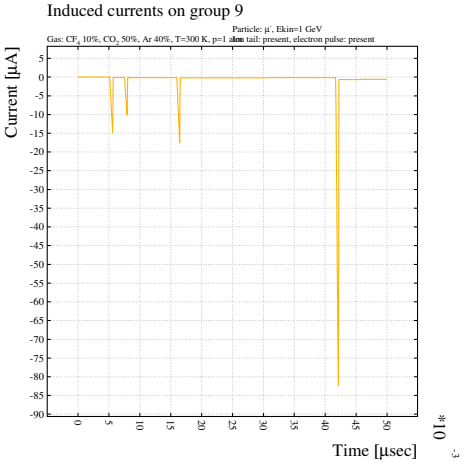

(d) Signal from wire-9

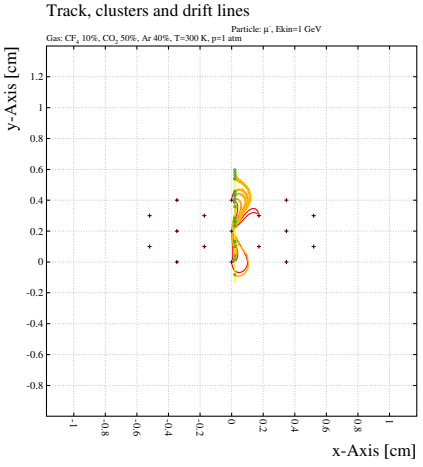

(e) Angle = 90°

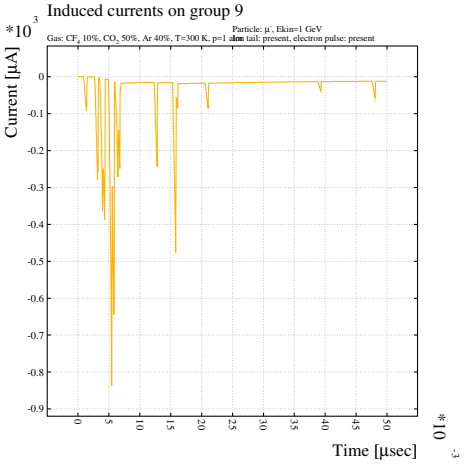

(f) Signal from wire-9

Figure 4.15: Track of the incoming muon of 1 GeV energy making various angle 45,60,90 to the x-axis of the detector geometry and the corresponding signal induced by ion-movement on central anode wire at 4000 V for $Ar/CO_2/CF_4$ (40/50/10) as the gas mixture

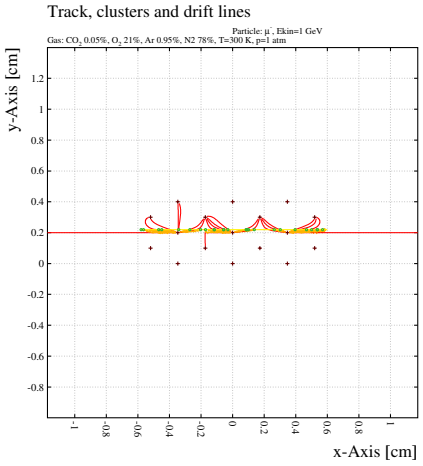

(a) Angle = 0°

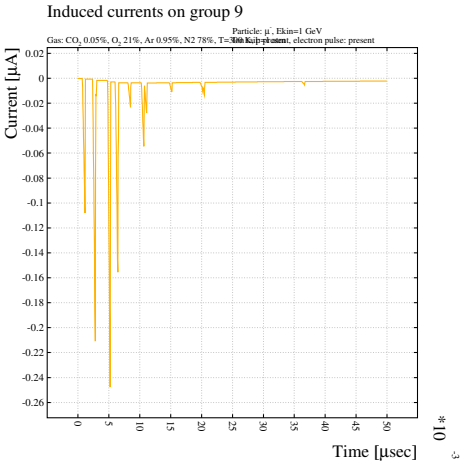

(b) Signal from wire-9

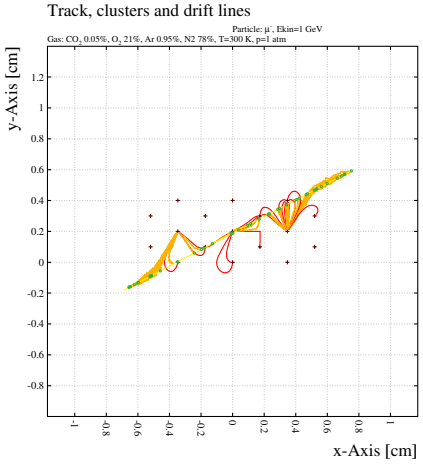

(c) Angle = 15°

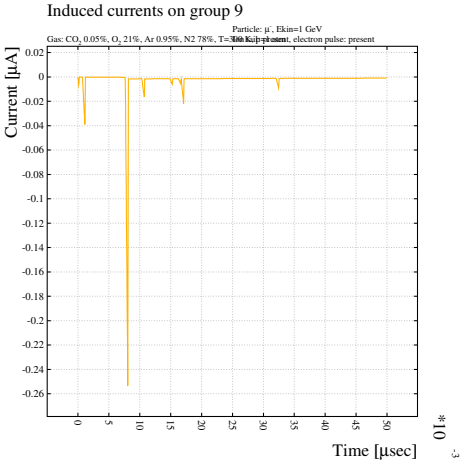

(d) Signal from wire-9

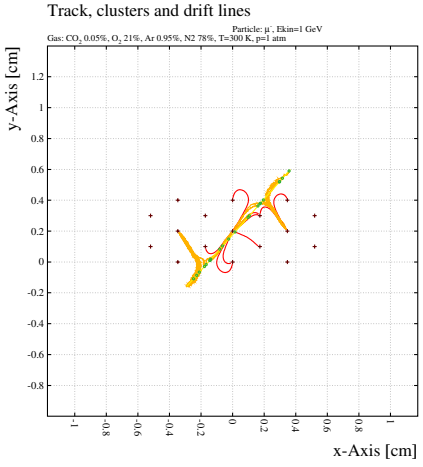

(e) Angle = 30°

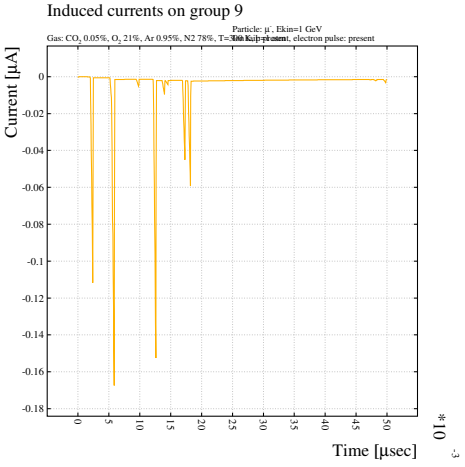

(f) Signal from wire-9

Figure 4.16: Track of the incoming muon of 1 GeV energy making various angle 0,15,30 to x-axis of the detector geometry and the corresponding signal induced by ion-movement on central anode wire at 4000 V for air as the gas mixture

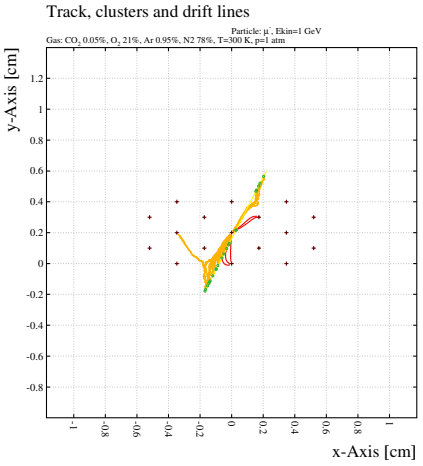

(a) Angle = 45°

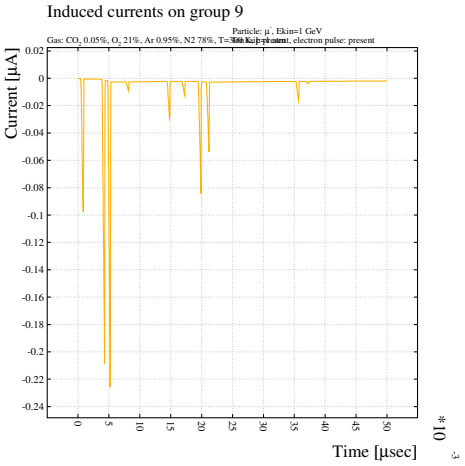

(b) Signal from wire-9

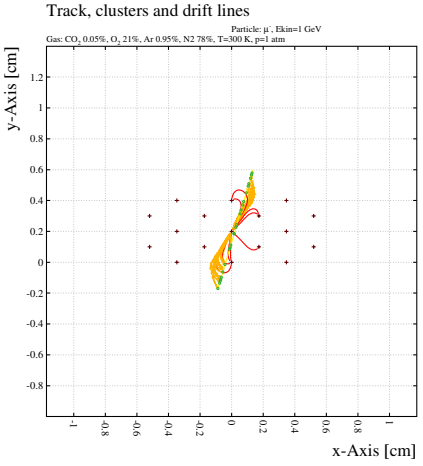

(c) Angle = 60°

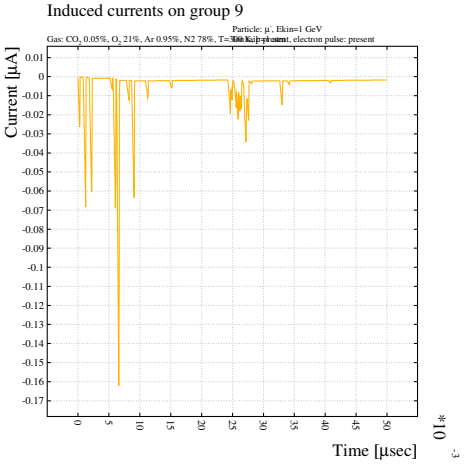

(d) Signal from wire-9

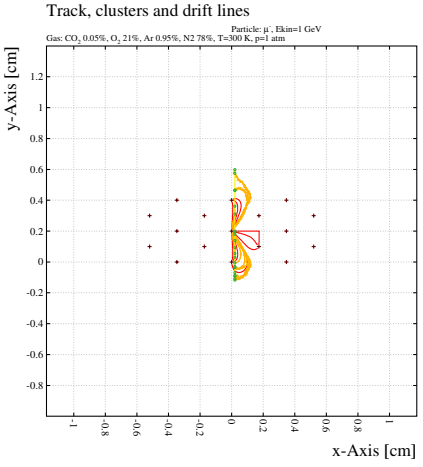

(e) Angle = 90°

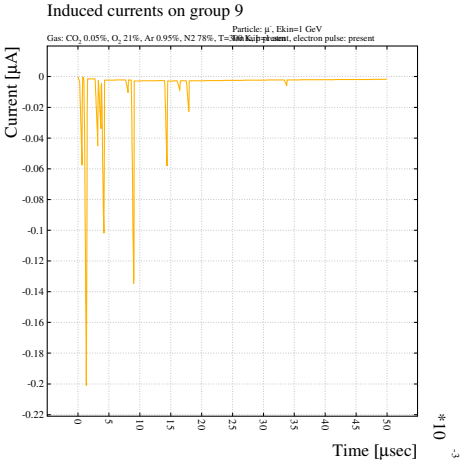

(f) Signal from wire-9

Figure 4.17: Track of the incoming muon of 1 GeV energy making various angle 45,60,90 to the x-axis of the detector geometry and the corresponding signal induced by ion-movement on central anode wire at 4000 V for air as the gas mixture

Chapter 5

Results and Discussion

We have done measurements with the muon of 1 GeV energy as the incoming particle and investigated the effect of inclined tracks on the timing resolution of the detector. The incoming particle when strikes the medium causes an avalanche effect near the anode where the electrons accumulate while the positively charged ions get deposited in the cathode. This initiates a current along the connected circuit. The anode is kept at a higher positive voltage (in our case 4000 V) while the cathode is kept at 0 V. The anode signal acts as a good timing signal while the cathode signal acts as the energy loss signal.

We observed the effect of inclination of the track w.r.t to one wire (which is the innermost middle wire of our geometry i.e. wire-9). The measurements were done with $Ar/CO_2/CF_4$ (40/50/10) gas mixture and were compared with that of air. The amplitude of the current on the anode was higher for $Ar/CO_2/CF_4$ as of air. The minimum time resolution implies a better detection efficiency and was obtained when the particle track was inclined at an angle 60° w.r.t x-axis. A time resolution of 0.26 ns at FWHM was obtained at 60° inclination for $Ar/CO_2/CF_4$ (40/50/10) gas mixture. But the current obtained on the wire for this inclination angle was minimum. Hence, there is a trade-off between observed current and time resolution. The best time resolution for 60° inclination was obtained because in this case the track of the particle is just seeing the innermost middle wire of the hexagonal arrays and all the electrons are getting collected at the wire-9. The trajectory of the incoming particle is far away from other wires and because of small drift path of electrons, most of the electrons are not reaching the other anode wires at high voltage. We obtained a sharp single peak for 60° inclination. In case of using air as the gas mixture, the best time resolution of 0.24 ns was obtained for 135° inclination w.r.t x-axis (angle measured

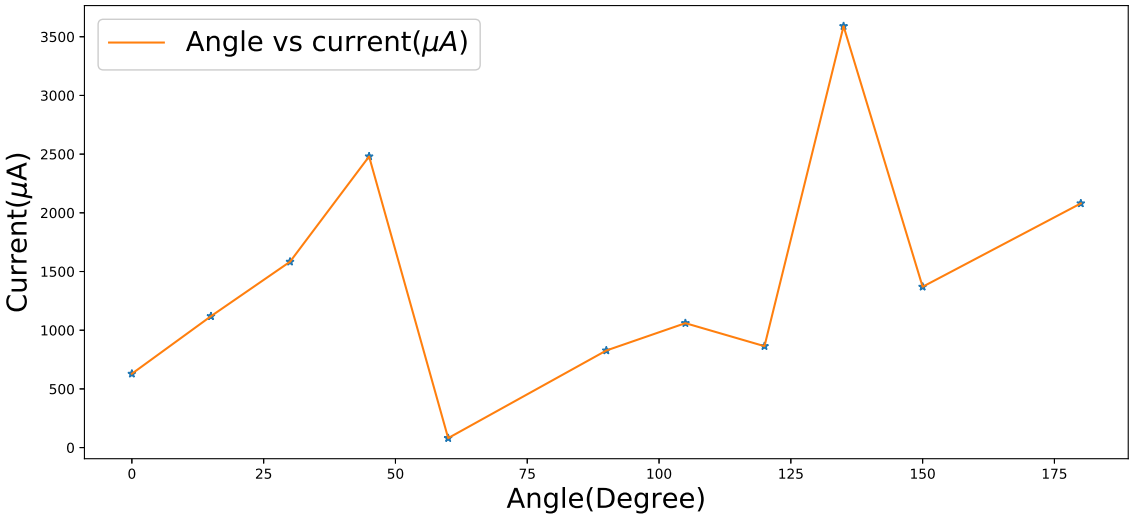

Figure 5.1: Simulated Time resolution versus current of the anode signal for $Ar/CO_2/CF_4$ (40/50/10) gas mixture

in an anti-clockwise direction). The only drawback of using air as the gas mixture is that the amplitude of current was very less of the orders of μA whereas in case of $Ar/CO_2/CF_4$ current it was of the order of mA. Air is, therefore, unsuitable for particle energy measurements. In contrast to the behavior with polyatomic molecules, an electron avalanche in air produces photons having long mean free paths caused by the small photon absorption in the air-these photons are eventually absorbed by the cathodes to eject photoelectrons. If the avalanche is sufficiently large, photoelectrons may be produced at the cathode surface which, in turn, contribute through additional multiplication to the total electronic charge collected at the center wire. Under these conditions, a space charge may form and the discharge will not be proportional to the original ionizing event. The gas amplification in the air is, therefore, limited to the region lying just above the proportional counting threshold and well below the incidence of photoelectrons. This limits air proportional counters to a maximum amplification of less than $5X10^2$, [29] above which the multiplication increases rapidly with relatively small increments of the applied potential. In contrast to this, polyatomic gases may employ gas amplification at least an order of magnitude greater. Among all the possible gases and gas mixtures that may be used in an MWPC, air must certainly be classed as a poor choice. However, the important advantages in using counters at atmospheric pressure with no windows or with windows having a high transmission for alpha-particles make this poor choice worthy of consideration.

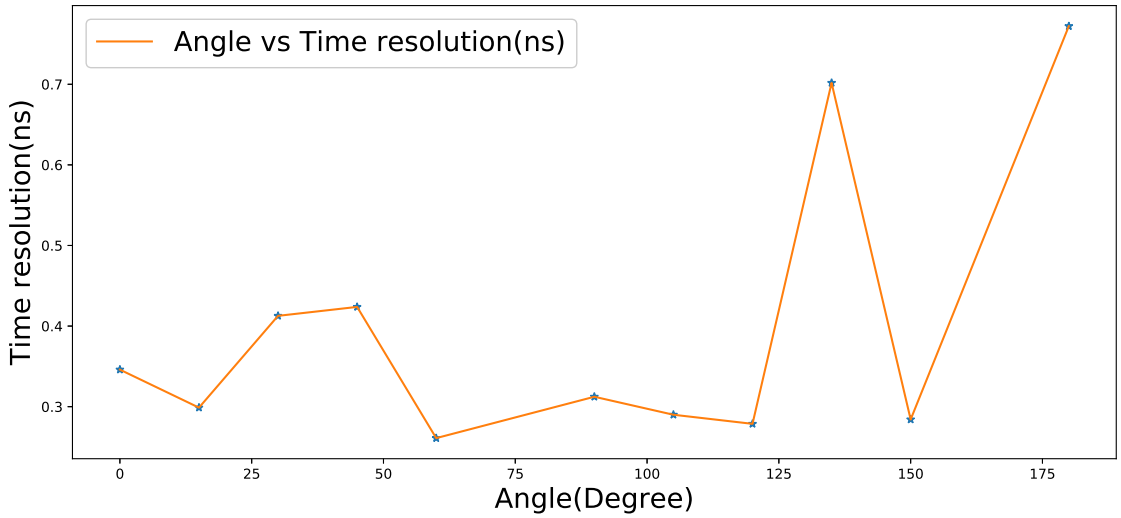

Figure 5.2: Simulated Time resolution versus the angle of the track of the incoming particle(muon 1 GeV) w.r.t x-axis for $Ar/CO_2/CF_4$ (40/50/10) gas mixture

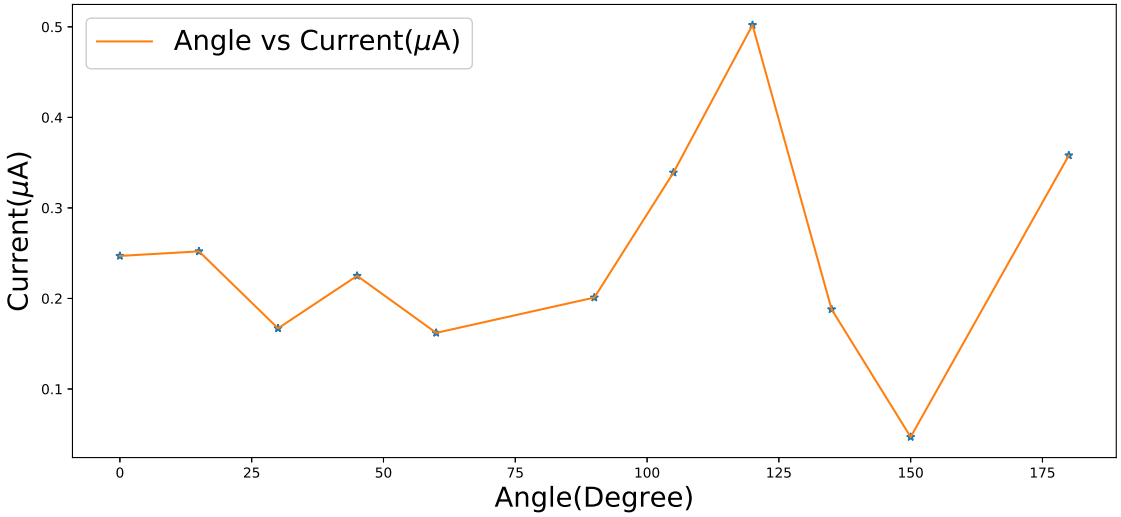

Figure 5.3: Simulated Time resolution versus current of the anode signal for air as the gas mixture

5.1 Summary and Conclusions

The subject of this thesis is the development of Air shower Multi-Mesh Proportional Counter. We have discussed the principles of the operational characteristics of MWPC and the mechanisms involved in radiation detection. This knowledge is necessary to

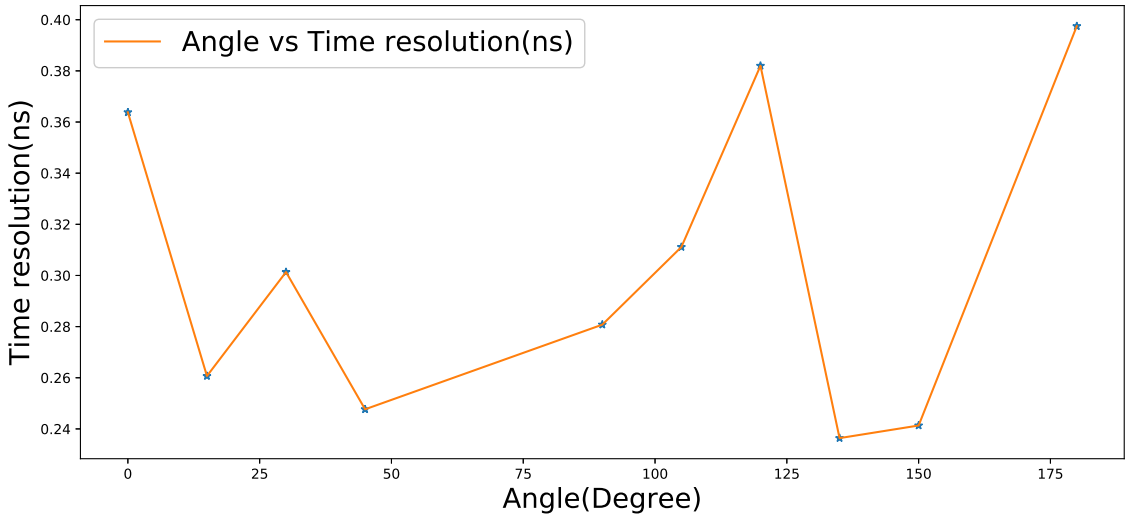

Figure 5.4: Simulated Time resolution versus the angle of the track of the incoming particle(muon 1 GeV) w.r.t x-axis for air as the gas mixture

understand and optimize the performance of the proposed detector. In our work, we have used the Garfield simulation framework for carrying out the simulation of the physical processes in MWPCs. The interface of Garfield with neBEM toolkit carried out 3D electrostatic field simulation for the proposed geometry. Besides neBEM, the Garfield framework provides interfaces to Magboltz for computing the transport and amplification properties of various gas mixtures. We have discussed about these simulation tools. To understand the software in detail, we have also presented some useful results using these tools. The optimal chamber operating conditions were calculated which gave maximum current (of the orders of mA) on the readout electrodes. The best time resolution (0.26 ns) was obtained at 60° inclination for $Ar/CO_2/CF_4$ (40/50/10) gas mixture. However, using air as the gas medium did not provide a detectable signal but this we can overcome by advancing the electronics which can detect signal of the orders of nV. Though our prime motivation was to make a large area detector which can be used in a cosmic ray air shower experiment, hence air being the cost effective solution is better alternative to the other specialized gas mixtures. Since the timing resolution obtained by using air is comparable with that of $Ar/CO_2/CF_4$, hence we can conclude that the air proportional counters are portable probes for the radiation detection and can be easily operated at atmospheric pressures. The only limitation is that we need a high operating voltage for air. High reactivity of other

gas mixtures as that of air would considerably limit the material lifetime of the material used for MWPC construction and also operating the detector at low gas pressure makes it more demanding to operate.

Bibliography

[1] W. Blum and L. Rolandi, *Particle Detection with Drift Chambers*. Springer-Verlag, 1993

[2] C. Grupen, *Physics of Particle Detection* Instrumentation in Elementary Particle Physics, Proceedings of the VII ICFA School, American Institute of Physics, edited by S. Kartal

[3] http://cern.ch/heed.

[4] http://garfield.web.cern.ch/garfield/

[5] http://magboltz.web.cern.ch/magboltz/

[6] G.Charpak, F.Sauli, *Multiwire proportional chambers and drift chambers* Nucl. Instrum. Methods 162 (1979) 405-428

[7] D. Groom, *Energy loss in matter by heavy particles* Particle Data Group Notes, PDG-93-06

[8] R. R. Roy and R. D. Reed, *Interaction of photons and leptons with matter* Academic Press, 1968

[9] Glenn F.Knoll *Radiation detection and measurement 4th ed.* New York, NY : Wiley, 2010. - 830 p.

[10] G. Charpak et al., *The use of multiwire proportional counters to select and localize charged particles*. Nucl. Instr. and Meth. **62** (1968) 262.

[11] *Time resolution limits of the MWPCs for the LHCb muon system* Nucl. Instr. and Meth. A 632(2011) 69-74.

[12] G.Charpak, D.Rahm, H.Steiner *Some developments in the operation of multiwire proportional chambers* Nucl. Instr. and Meth. 80(1970) 13-34.

[13] Dezs Varga et al., *Cosmic Muon Detector Using Proportional Chambers* 2015 Eur. J. Phys. 36 065006.

[14] H. Natori et al., *A Fast High-Voltage Switching Multiwire Proportional Chamber* `arXiv:1612.08329`

[15] Archana Sharma, *Properties of some gas mixtures used in tracking detectors.* SLAC-JOURNAL-ICFA-16-3, 1998.

[16] L.G.Christophorou, D.L.McCorkle, D.V.Maxey, J.G.Carter *Fast gas mixtures for gas-filled particle detectors* Nucl. Instr. and Meth. 163 (1979) 141-149

[17] A. Peisert and F. Sauli, *Drift and diffusion of electrons in gases: compilation* CERN report, 84-08 (1984).

[18] R. Veenhof, *GARFIELD: simulation program for gaseous detectors.*

[19] Y.Sakai, H. Tagashira and S.Sakamoto, *The development of electron avalanches in argon at high E/N values: I. MonteCarlo simulation* J. Phys D: Appl. Phys., 10 (1977) 1035

[20] T. Itoh and T. Musha, *Monte Carlo Calculations of Motion of Electrons in Helium* J. Phys. Soc. Japan 15 (1960) 1675

[21] S.Mukhopadhyay, N.Majumdar, *Proceedings of ICCES'05,* TechScience Press (2005).

[22] S.Mukhopadhyay, N.Majumdar, *Engg Analysis Boun Elem, 30,* pp.687-696 (2006).

[23] N. Majumdar, S. Mukhopadhyay, *Simulation of three-dimensional electrostatic field configuration in wire chambers: A novel approach* Nucl. Instr. and Meth. A 566 (2006) 489494.

[24] N. Majumdar and S. Mukhopadhay, *nearly exact Boundary Element Method,* `http://cern.ch/nebem(2009).`

[25] R. Veenhof, *Nucl. Instr. and Meth. A 419 (1998) 726.*

[26] G.A. Erskine, *Electrostatic Problems in Multiwire Proportional Chambers,* Nucl. Instr. Meth. 105 (1972) 56572

[27] L.J. Koester, et al., *Measurements of Efficiency and Time Resolution of Multiwire Proportional Counters,* Nucl. Instr. Meth. 82, 67 (1970).

[28] P.Bhattacharya et al., *Detailed 3D Simulation of the GEM-based detector,* Journal of Physics: Conference Series 759 (2016) 012071.

[29] J. A. Simpson Jr., *Air Proportional Counters,* Review of Scientific Instruments 19, 733 (1948).